



Qualification of innovative floating substructures for 10MW wind turbines and water depths greater than 50m

Project acronym LIFES50+
Grant agreement 640741
Collaborative project
Start date 2015-06-01
Duration 40 months

Deliverable **D4.3 Optimization framework and methodology for optimized floater design**

Lead Beneficiary USTUTT
Due date 2016-12-30
Delivery date 2016-12-30
Dissemination level Public
Status Final
Classification Unrestricted

Keywords Floating offshore wind turbine, optimization, modelling
Company document number [Click here to enter text.](#)



The research leading to these results has received funding from the European Union Horizon2020 programme under the agreement H2020-LCE-2014-1-640741.

Disclaimer

The content of the publication herein is the sole responsibility of the publishers and it does not necessarily represent the views expressed by the European Commission or its services.

While the information contained in the documents is believed to be accurate, the authors(s) or any other participant in the LIFES50+ consortium make no warranty of any kind with regard to this material including, but not limited to the implied warranties of merchantability and fitness for a particular purpose.

Neither the LIFES50+ Consortium nor any of its members, their officers, employees or agents shall be responsible or liable in negligence or otherwise howsoever in respect of any inaccuracy or omission herein.

Without derogating from the generality of the foregoing neither the LIFES50+ Consortium nor any of its members, their officers, employees or agents shall be liable for any direct or indirect or consequential loss or damage caused by or arising from any information advice or inaccuracy or omission herein.

Document information

Version	Date	Description
01	2016-11-04	Draft
		Prepared by Kolja Müller, Frank Lemmer, Wei Yu, Ricardo Faerron Guzman
		Reviewed by Enter names
		Approved by Enter names
02	2016-12-09	Draft for review
		Prepared by Frank Lemmer, Kolja Müller, Wei Yu, Ricardo Faerron Guzman, Matthias Kretschmer
		Reviewed by Marco Belloli, Ilmas Bayati, Denis Matha
		Approved by
03	2016-12-29	Final
		Prepared by Frank Lemmer, Kolja Müller, Wei Yu, Ricardo Faerron Guzman, Matthias Kretschmer
		Reviewed by Jan Norbeck
		Approved by Petter Andreas Berthelsen
In order to enter a new version row, copy the above and paste into left most cell.		

Authors	Organization
Frank Lemmer	USTUTT
Kolja Müller	USTUTT
Wei Yu	USTUTT
Ricardo Faerron Guzman	USTUTT
Matthias Kretschmer	USTUTT

Contributors	Organization
David Schlipf	USTUTT
Friedemann Borisade	USTUTT
Henrik Bredmose	DTU
Michael Borg	DTU



Definitions & Abbreviations

1p	One time per rotor revolution
3p	Three times per rotor revolution
AeroDyn	Aerodynamic simulation model by NREL
ANN	Artificial Neural Network
APDL	Ansys Parametric Design Language
AQWA	Potential flow simulation model by Ansys
BEM	Blade Element Momentum
Bladed	Aero-hydro-servo-elastic simulation model by DNV-GL
BldPch	Blade Pitch
CAPEX	Capital Expenditures
CPU	Central Processing Unit
DEL	Damage-Equivalent Load
DLC	Design Load Case
DoE	Design of Experiments
DOF	Degree Of Freedom
DTU	Technical University of Denmark
DTU10MW	DTU 10 MW Reference Wind Turbine
EOG	Extreme Operational Gust
EQM	Equations of Motion
FAST	Aero-hydro-servo-elastic simulation model by NREL
FEM	Finite Element Model
FFT	Fast Fourier Transform
FLS	Fatigue Limit State
FOWT	Floating Offshore Wind Turbine
GA	Genetic Algorithm
GA	Genetic Algorithm (Optimizer)
GenTq	Generator Torque
HAWC2	Aero-hydro-servo-elastic simulation model by DTU
LCOE	Levelized cost of energy
LHS	Lattice Hypercube Samples
LHS	Latin Hypercube Sampling
LQ	Linear Quadratic
LQR	Linear Quadratic Regulator
MATLAB	Software from Mathworks
MDAO	Multi-Disciplinary Design and Optimization
MIMO	Multiple-Input-Multiple-Output
MSL	Mean Sea Level
NMPC	Nonlinear model-predictive control
NREL	National Renewable Energy Laboratory
O&M	Operation & Maintenance
OC3	Offshore Code Comparison Collaboration
OC4	Offshore Code Comparison Collaboration Continuation
OC5	Offshore Code Comparison Collaboration Continuation with Correlation
ODE	Ordinary Differential Equation
PI	Proportional-Integral (controller)
PitchPos	Platform Pitch Position
PitchVel	Platform Pitch Velocity
PS	Particle Swarm (Optimizer)
PSD	Power spectral density
PSO	Particle Swarm Optimizer
RAO	Response Amplitude Operator

RNA	Rotor-nacelle assembly
RotSpeed	Rotor Speed
RWT	Reference Wind Turbine
SIMA	Floating systems simulation model by MARINTEK
Simpack	Multibody simulation tool by Dassault
SISO	Single-Input-Single-Output
SLOW	Simplified Low-Order Wind turbine (simplified model by USTUTT)
SoA	State-of-the-Art
STD	Standard Deviation
SurgePos	Surge Position
SurgeVel	Surge Velocity
SWE	Stuttgart Wind Energy
SWL	Sea Water Level
TLP	Tension Leg Platform
TSR	Tip-Speed Ratio
TwrTopPos	Tower Top Position
TwrTopVel	Tower Top Velocity
ULS	Ultimate Limit State
WAMIT	Wave analysis simulation model by MIT
WP	Work Package

Symbols

$A(\omega)$	Added mass matrix
A_c	Added mass interpolated at eigenfrequencies
a	Artificial Neural Network output vector
$B(\omega)$	Potential flow damping matrix
B	Linear time-invariant model input (SLOW)
b	Artificial Neural Network biases
C	Hydrostatic restoring matrix
c_P, c_T	Aerodynamic power and thrust coefficients
d	Semi-submersible column spacing (distance from centreline)
d_i	Estimated linear hydrodynamic damping coefficient
dt	Time step
E	Identity matrix
F_{aero}	Aerodynamic thrust force
$F_{exc}(\omega)$	Hydrodynamic wave excitation force
f	Frequency; function of ...
f_p	Peak spectral frequency
H_F, V_F	Horizontal and vertical fairleads forces
H_s	Significant wave height
h_{hp}	Semi-submersible heave plate thickness
i	Imaginary unit
J	Cost function (for optimization)
K_{lqr}	Linear quadratic regulator state feedback gain matrix
k	Applied forces
M	Structural mass matrix
M_g	Generator torque
M_{aero}	Aerodynamic torque
P	Linearized velocity-dependent forces
p	Coriolis, centrifugal and gyroscopic forces
q	Generalized coordinates
Q_c	Linear quadratic regulator weight matrix on states

\mathbf{Q}	Linearized position-dependent forces
\mathbf{R}_c	Linear quadratic regulator weight matrix on inputs
R	Rotor radius
r	Semi-submersible column radius
$\hat{r}_{hp}, \hat{r}_{hp,in}$	Semi-submersible heave plate radius to column radius ratio; desired value
$\dot{r}_{rotor,x}$	Horizontal hub velocity
s	Laplace variable
s	Artificial Neural Network number of neurons
T_p	Peak spectral period
t	Time
\mathbf{u}_0	Input set point
$\Delta \mathbf{u}$	Differential model input
$\mathbf{X}(\omega)$	Wave excitation force coefficient
$\mathbf{x}(t)$	State vector
\mathbf{x}_0	State set point
$x_p(t)$	Platform surge displacement
$x_t(t)$	Tower-top fore-aft displacement
$v_0(t)$	Rotor-effective wind speed/Mean wind speed
v_{rel}	Relative rotor-effective wind speed
\mathbf{W}_p	Artificial Neural Network neuron-specific weighted inputs
x_F, z_F	Horizontal and vertical fairlead displacement
$z_p(t)$	Platform heave displacement
$\beta_p(t)$	Platform pitch displacement
$\eta_0(t), \tilde{\eta}(\omega)$	Wave elevation at platform initial position, wave height spectrum
$\theta(t)$	Blade pitch angle
λ	Tip-speed ratio (TSR)
ξ	Generalized rigid-body coordinates of floating body
ρ	Density
ω	Angular frequency
$\Omega(t)$	Rotor speed
Ω_{rated}	Reference (rated) rotor speed

Executive Summary

Floating offshore wind turbines are complex dynamic systems. The optimization in terms of cost and dynamic behavior is the focus of the present report, which is part of Subtask 4.1.3 of the LIFES50+ project. Subject to the optimization is the floating platform hull shape while adapting the wind turbine controller to the properties of the platform in every optimization loop. The framework includes several simulation codes and design scripts including a parameterized hydrodynamic panel code and a simplified coupled floating offshore wind turbine model. The methodology assist the designer in the early design stages (i.e. conceptual design and basic design) to focus on the most feasible solutions from the beginning and thus speed up the overall design process.

The simplified model is an essential part of the framework, as the numerous iterations that are part of an optimization procedure require a sufficiently small runtime. The model consists of a nonlinear multibody system, which can be easily adjusted for new layouts of the floating wind turbine and platform. The efficient modeling results in a short simulation time (around 160 times faster than real time on a standard PC), which enables the designer to run many system simulations and sensitivity studies early in the design and hence is also ideally suited for optimization applications. The model can be linearized for even faster frequency domain evaluations or control design approaches.

In this study, the SWE-TripleSpar was evaluated, a publicly available, generic semi-submersible concrete platform, on top of which the DTU10MW reference turbine is positioned. The four design parameters, which are chosen as independent variables in this work, are (1) the column spacing and (2) the platform radius, (3) the heave plate height and (4) the ratio of heave plate and column radius. The implemented controller is an optimal, model-based controller, which has the advantage that the gains are calculated based on the linearized state-space model such that a tailored controller results for every new hull shape. For the design evaluation, a simplified set of power production load cases is used, based on the LIFES50+ site B (GFOlf of Maine) design basis description. Extreme load cases are only roughly considered in the structural pre-dimensioning. The dynamics during power production are the focus of the report.

Before the optimization a design space exploration was done based on a Design of Experiment methodology in order to verify the appropriate definition of the free variables, the free variable bounds, the cost function and the subsystem design assumptions. For the selection of the optimizer, a metamodel based on an Artificial Neural Network fit is applied in order to find the algorithm with the least necessary iteration and its settings.

The pattern search algorithm was selected due to the nonlinear and non-differentiable problem at hand. The algorithm is also capable of considering known and unknown hard constraints. The chosen cost function takes into account the material cost of the substructure as well as the dynamic loads of the system.

Results show that optimization can help finding well suited solutions for a given site given that sufficient time is put in careful preparation, definition and evaluation of the overall optimization procedure. For the applied combination of site and cost function, the initially included heave plates turned out to be able to reduce the response to waves but at the cost of increased material usage. Two optimization runs with different cost functions reveal the implications of realizing a maximum possible cancellation of wave forces.



Contents

1	Introduction	8
1.1	Scope	10
1.2	Methodology	11
2	Modelling Approaches and Assumptions.....	14
2.1	Hydrodynamics	15
2.2	Mooring dynamics.....	16
2.3	Aerodynamics.....	17
2.4	Reduced-order simulation model SLOW	18
2.5	Control.....	19
3	Optimization framework	20
3.1	Design of Experiments	20
3.2	Optimization variables	22
3.3	Design Space	23
3.4	Platform structural design assumptions.....	24
3.5	Hydrostatics and hydrodynamics	26
3.6	Mooring design.....	27
3.7	Linear Model	28
3.8	Controller.....	28
3.9	Coupled SLOW simulations.....	29
3.10	Load cases	29
3.11	System Optimization	30
4	Results and Discussion	32
4.2	Full system optimization	36
5	Conclusion.....	40
6	Outlook.....	40
7	Appendix	42
7.1	Evaluation of optimization algorithms	42
8	Bibliography	48

1 Introduction

The task of designing a substructure for floating offshore wind turbines (FOWT) is a multidisciplinary problem. In LIFES50+ many of the design-driving aspects are being analysed, especially in WP2, in which the performance of the different FOWT platform concepts is evaluated. From a certification point of view the structural integrity, stability, safety and lifetime are a main concern. Here, numerical simulation models represent the complex aero-hydro-servo-elastic nature of the system. The major components are the mooring lines, the platform, the tower and the rotor-nacelle-assembly. These components face different environmental loads, which are modelled individually and with varying level of detail, see LIFES50+ D4.4 (Borg and Bredmose, LIFES50+ D4.4 Overview of the numerical models used in the consortium and their qualification 2015). Hence, the early design is typically done in iterative steps and with differing level of detail for the different components of the floating platform. An essential part of this procedure is to focus on the main hull shape dimensions early in the design and apply adjustments later in the design if important requirements are not met. The herein presented optimization framework is developed as a tool supporting the designers in the conceptual design stage. The optimization objectives of this multidisciplinary problem are reduced for this task in order to meet the range of validity of the simplified simulation models and to still allow the designer to define the constraints due to manufacturing, transport and installation requirements, which are not directly included in the presented models. This will lead to feasible optima from a point of view of the dynamic behaviour still involving the experience from earlier projects represented through constraints. However, a system engineering approach looking at the whole system already in the conceptual design stage is the objective of this work in order to streamline the design process of FOWT. A design practice for FOWT with three stages (conceptual design, basic design and detailed design) was developed in LIFES50+ D7.4 (Müller, Lemmer, et al. 2015).

This report focuses on parameterized and computationally efficient numerical simulation models to represent the dynamic behaviour of the system. This builds up on the reduced-order numerical models that were presented in LIFES50+ D4.1 (Lemmer, Müller, et al. 2016) that enable the designer to quickly evaluate a given design on the base of time domain analyses. Thus, the presented models also allow an evaluation of how a considered design will behave dynamically in a given environment, next to the typically performed “spreadsheet” design process looking at the static integrity and stability. Hence, the simple models are ideally suited for an advanced design optimization in the early design of FOWT systems. A more detailed, high-fidelity evaluation of a large number of designs at the conceptual stage of the design is difficult to include due to the numerical effort required by state-of-the-art tools for time domain analysis, which is required for a more detailed investigation of the system behaviour.

One of the main efforts in the LIFES50+ project is the technologically viable upscaling of existing substructure concepts for FOWTs from 5MW to 10MW systems (subtask 4.1.2). The optimization methodology presented is applied to a concrete semi-submersible concept. Its main parameters and assumptions are derived from the publicly available design (Lemmer, Amann, et al. 2016), which was originally developed in the project INNWIND.EU, see (Sandner, Yu and Matha, et al. 2014) and further developed for LIFES50+ D4.1, (Lemmer, Müller, et al. 2016) because the public upscaled LIFES50+ designs are not yet available. However the developed and herein presented approach is suitable to be applied to any of the four LIFES50+ designs, and will, in a later project stage, also support the upscaling of the selected substructures. The environmental conditions for the design load calculations (DLC), especially DLC 1.2 are taken from the LIFES50+ Design Basis (Gómez Alonso, et al. 2015). In particular, the environmental conditions of Site B – Gulf of Maine were considered in this work.



Design optimization is a topic in engineering which has been addressed extensively in the literature. A comprehensive study on hull shape and mooring line optimization of FOWT across different platform types using a genetic algorithm was done by (Hall, Buckham and Crawford 2013). Here, a frequency-domain model is derived from the code FAST (Jonkman and Buhl, Fast User's Guide 2005) with a linear representation of the hydrodynamic viscous damping but without representing the wind turbine control. The genetic algorithm is applied for single- and multi-objective optimization. The results show different rather un-conventional designs which might indicate that a refinement of the cost function is necessary. Another work on optimization of FOWT using a spar-type platform is presented in (Fylling and Berthelsen 2011). It includes the mooring lines and the power cable but does not include the dynamics of the wind turbine and the control. The results show that the response can be optimized by modifying the cylindrical shape of a spar. Another integrated optimization approach for spar-type FOWT using the multi-body code Simpack was presented in (Härer, et al. 2013) and in (Sandner, Schlipf, et al., Integrated Optimization Of Floating Wind Turbine Systems 2014) comparing three spar-type platforms with tailored blade-pitch controllers. A parametric study of a semi-submersible platform for design optimization can be found in (Aubault, Cermelli and Roddier 2007) and another work specific to TLPs is part of the thesis (Bachynski 2014). Here, especially hydrodynamic loading of first, second and third order is considered with the combination of the controller and controller faults in extreme sea states. Another work on TLP optimization for load reduction can be found in (Myhr and Nygaard 2012). Examples for optimization studies are presented in the thesis (Kühn 2003), which addressed integrated design and optimization of offshore wind turbines and in (Häfele and Rolfes 2016), where a Particle Swarm Optimizer (PSO) was applied to jacket substructures. A comparable study with a Genetic Algorithm (GA) was presented in (Schafhirt, Zwick and Muskulus 2014). And a short overview of a monopile and jacket optimization can be found in (Ruiter 2015). A gradient-based optimizer was applied for offshore support structures in (Chew, Tai and Muskulus 2015). With this optimizer it is especially important to ensure a continuous description of the cost function. An example for a parametric design model of oil & gas support structures subject to optimization for a reduced downtime through improved seakeeping is given in (Birk, Clauss and Lee 2004). Optimization studies have also been done for the mooring lines of FOWT, see (Brommundt, et al. 2012). Also, an example of optimization of mechanical systems using multibody approaches from a more theoretical viewpoint can be found in the thesis (Kurz 2013).

Specifically new to this study is the inclusion of the wind turbine controller within the optimization in order to investigate the effect of varying aerodynamic damping through the coupled dynamics of the blade pitch and the generator torque controller during operation. It was shown in (Fleming, Peiffer and Schlipf 2016) and (Lemmer, Schlipf and Cheng 2016) that it is difficult for semi-submersibles to mitigate first-order wave loads with the wind turbine controller due to the limited control authority, or limited effect of the actuators blade pitch angle and generator torque compared to the effect of wind and wave loads. Especially the blade pitch control design is a challenge for floating wind turbines because of the low-frequency dynamics of the support structure. These introduce an inverse-response behaviour of the control due to the interaction of the fore-aft motion with the control, which results in a “negative damping” of the FOWT system. This has been described in (J. Jonkman, Influence of Control on the Pitch Damping of a Floating Wind Turbine 2008) for conventional single-input-single-output control and recently in (Fischer and Loepelmann 2016) for an improved behaviour using more control inputs than the rotor speed error. Another example of advanced controllers for FOWTs using wind preview information is (Schlipf, Simley, et al. 2015). In the latter study an optimal controller is applied, which is based on a linear dynamic model of the system. This has been applied for FOWT before and was presented among others in (Lemmer, Raach, et al. 2015), (Raach, et al. 2014) and (Lindeberg 2009). For this work the control architecture was selected such that its design depends on

the actual dynamics of the current platform geometry for a parametric definition within the optimization loop. An optimal Linear Quadratic Regulator (LQR) is defined for each platform design iteration using a linear model and applying the same cost function for all platforms in order to allow a “fair” comparison between the different solutions. Consequently, a design will not be disregarded only due to a suboptimal controller. The optimal controller results in the upper bound of what is possible to achieve with control. This causes the optimizer to adjust the hull shape for a further improvement of the response where the effect of the control reaches its limit.

In the design, additional input needs to be considered from a number of disciplines that play a major role in different parts of the system lifetime (e.g. engineering, production & logistics, maintenance, economics, risk analysis, etc.). Essentially all of these disciplines have an influence on the resulting LCOE of the regarded system. Hence, when looking for an optimal design it is necessary to take into account the manifold interests that will play a role in the decisions. As mentioned previously, these aspects are considered a part of the experience of the design engineers and are not part of the presented framework. This early-stage system engineering analysis will be, fed with the definitions and bounds by the designer, a useful support in the design process. The result is a platform hull shape with given requirements and constraints, available at the conceptual design stage. This shape will give the basis for more advanced design analyses, which are expected to introduce further minor modifications of the system. A summary of the scope of the report is given in the next section before the methodology will be described in detail.

1.1 Scope

The main objective of this study is to provide a valid optimization methodology with efficient simplified simulation models still producing reliable results for the considered load cases with an adequate cost function and a first application of the method. A summary of the focus and the limitations of the study is given in the following:

- **Optimization focuses on the semi-submersible substructure concept with geometric parameters as optimization variables**

The optimization focuses on a three-column semi-submersible with catenary mooring lines and does not include other types of FOWT concepts (TLP, barge, spar). In comparison to previous work, this means rather small variations around a given baseline geometry including the engineers experience and know-how. The DTU10MW turbine of LIFES50+ D1.2 is applied and not modified, except for the controller. The platform main parameters are those of the SWE-TripleSpar concept already applied in LIFES50+ D4.1. An extension to other platform types is possible.

- **Platform specific controller design is included in each iteration.**

The controller is an essential part to be included in the optimization loop as it has a significant influence on the overall system behavior in operational conditions. Including an optimal controller in each design, iteration means to apply a fair comparison between iterations. This has not been done in previous optimization publications and allows an assessment of the design alterations induced by the controller. The applied controller does not include observers and sensor models in order to focus on the hull shape geometry with the best possible controller, assuming perfect measurements of the states.

- **The optimization is intended to be applicable in the conceptual design stage**

The main geometric sizing shall be determined through the optimization. This means that simplified models are used, focusing on first-order loads and neglecting higher-order dynamics. The design is expected to change slightly during the subsequent design stages.

- **The optimization focuses on the rejection of wind and wave excitation in operational conditions.**

Power production is the situation faced most of the time by the system and is hence taken to be the base for the evaluation of the design for a minimum motion response during operation, including only an estimate of the extreme loads. The simplified simulation models applied in this work can efficiently and with sufficient accuracy describe the system behaviour in operational conditions. Structural design for ULS is expected to be part of the following design stages. This contradicts the current design procedure, which focuses on ULS first, mostly due to the fact that full wind turbine models are not available to the offshore engineers, see (Müller, Lemmer, et al. 2015).

- **Different optimization algorithms and design space explorations are assessed**

For an understanding of the problem set, a valid selection of free variables and the cost function a design space exploration using Design of Experiments (DoE) was done before different optimizers were assessed. In this work, optimization functions which are implemented in MATLAB have been investigated: *gradient based, pattern search and particle swarm*.

- **The optimization framework does not include the disciplines of manufacturing, installation, O&M.**

Constraints related to e.g. transportation, manufacturability, etc. are expected to be determined by the design engineer and are not part of the automated optimization routine.

Following these limitations, the presented framework aims to provide feasible initial designs for a new site to be considered, based on an initial, parameterized geometry.

1.2 Methodology

The requirements for the presented optimization framework are

- the computational efficiency of the simulation models
- the indicative prediction of the dynamic response and loads (ULS and FLS) of the system with given environmental conditions.

The goal is the definition of a hull shape and controller in order to obtain:

- a maximum reduction of the response to wind and waves, meaning a smooth power production
- reduced structural fatigue loads for an extended lifetime.

This is expected to result in a reduced Levelized Cost of Energy (LCOE) of the detailed design. The presented framework is implemented as part of a simulation toolbox written in MATLAB. The core part is a combination of a parametrized subsystem design and the simplified FOWT model SLOW (Simplified Low-Order Wind turbine), which is presented in Chapter 2. The overall workflow is shown in Figure 1.

Numerical optimization using a mathematical problem formulation is usually applied for interconnected systems, hard to overlook by the designer. Multi-disciplinary design & optimization (MDAO), suc-

cessfully applied to wind turbine systems can incorporate multi-physics simulation codes and multi-dimensional cost functions. Here, the complexity introduced through the different fields needs to be accurately represented by the mathematical model. If only a scalar cost function is applied then the optimization can help to find the optimal tradeoff, often involving a number of contradicting design objectives. In this study, an optimizer is applied due to the complex dynamic behavior of FOWT, governed by stochastic wind and wave excitations combined with nonlinear structural and controller behavior, which is difficult to interpret using simple correlations. The first-order wave excitation forces, for example, depend on the hull shape geometry, but the addition of all force components with different phases and their impact on the coupled overall system dynamics including the wind turbine is a highly nonlinear problem; similar complexity applies to the aerodynamic forces from turbulent wind as well. This is the reason why an optimizer and a mathematical problem formulation is applied here.

In order to reduce the complexity of the optimization the number of free variables was set to a minimum. This means that the designer is expected to define clear bounds of feasible concepts. The design space will be a combination of hull shape parameters, while the wind turbine is unchanged, except for the blade-pitch and generator torque control. The model used is the DTU10MW reference wind turbine, described in LIFES50+ D1.2 (Borg and Bredmose, LIFES50+ D1.2 Wind turbine models for the design 2015) and (Bak, et al. 2013). In the presented framework a variety of design parameters are functions of the free variables. This means that an automated design of the components based on the free variables is done. This is called “subsystem design” and is included in the optimization algorithm, see Figure 1. Especially the preliminary structural design and the control design are done within subsystem design routines. An internal root-finding algorithm determines one of the hull shape parameters based on the constraint of the static pitch angle of the platform under the thrust force at rated wind speed. This constraint ensures the linear hydrostatic restoring and therefore the stability of the system as well as the rotor misalignment with the wind and therefore the cosine-losses of the produced power. This approach has already been applied in (Sandner, Yu and Matha, et al. 2014). The first step for setting up the optimization problem is the determination of the chosen free variables and the bounds which allow designs that meet the static pitch angle constraint. The optimization loop feeds these into the subsystem design procedure, where the structural dimensioning based on assumed ULS stresses is made and the mooring lines are designed, see Section 2.2. The interface between these submodules is a data structure in Matlab, which is the driving software. Once the system design is established, the hydrodynamic characteristics of the platform are determined through panel code simulations, Section 2.1. With this information a system transformation is necessary to provide the input files for the simulation model. In a first step, the steady state of the system is determined through a nonlinear time-domain simulation for all operational wind speeds at still water. Subsequently, linear models are derived for the same wind speeds, Section 2.4. These models are the basis for the design of an optimal model-based controller for each of the designs. This controller includes an optimization using determined weighted cost functions for the response of the states and the actuators, see Section 2.5. This procedure ensures that a concept is not discarded due to suboptimal settings of the controller as the cost function for the control design is the same for all designs. The resulting system properties are then handed over to the nonlinear SLOW model, which simulates the time-domain system response for defined environmental conditions. The results are then post-processed and combined in a cost function and transferred back to the optimization algorithm which chooses the next combination of free variables, see Section 3.11.

The cost function is a function of the outputs of the routines called within the optimization loop marked in dark blue in Figure 1. The outputs of the routines marked with lighter blue are the ones that the subsequent routines need for the further design calculations and simulations.



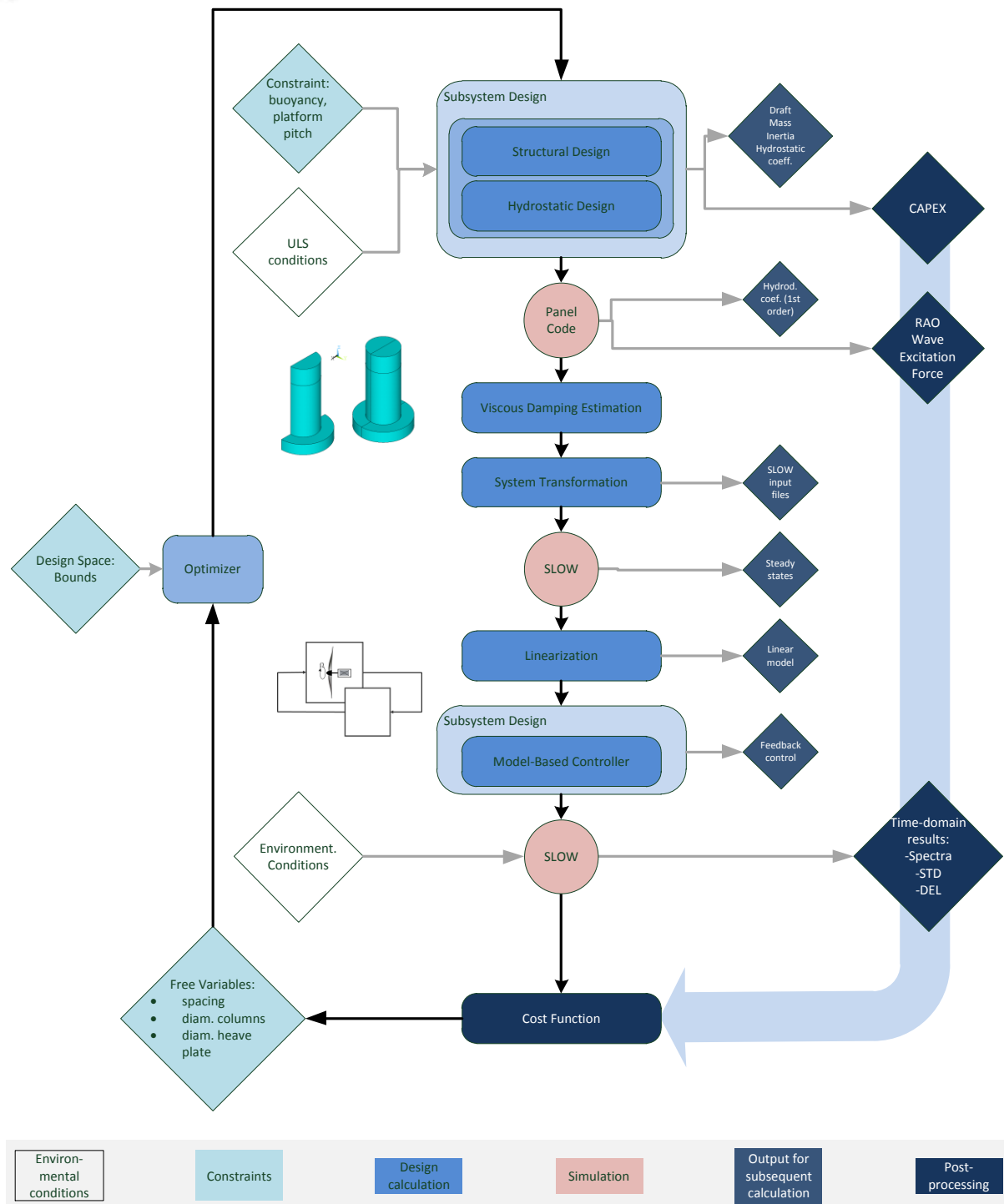


Figure 1: Workflow of optimization procedure

2 Modelling Approaches and Assumptions

Since even the simple models do not run fast enough to do a fully integrated optimization, the applied framework comprises a mix of various reduced-order models available for the design and design evaluation of FOWT systems. These enable the capturing of all relevant physical effects within acceptable accuracy. Within the optimization, a de-coupled design of the substructure is performed both by a static analysis based on analytical equations as well as by a hydrodynamic panel code analysis in fre-

quency domain, see Figure 1. The results of these analyses are inputs to the SLOW (Simplified Low-Order Wind turbine) model in preparation for time-domain simulations, which are conducted after the controller has been defined for the final system evaluation. The simplified FOWT model SLOW developed at the University of Stuttgart allows a fast simulation of the overall nonlinear coupled dynamics and is also explained in more detail in LIFES50+ D4.1 (Lemmer, Müller, et al. 2016), (Sandner, Schlipf, et al., Reduced Nonlinear Model of a Spar-Mounted Floating Wind Turbine 2012) and (Matha, Sandner and Schlipf, Efficient critical design load case identification for floating offshore wind turbines with a reduced nonlinear model 2014).

2.1 Hydrodynamics

The complete hydrodynamic model includes the linearized hydrostatics through the hydrostatic restoring matrix \mathbf{C} , which is, prior to the hydrodynamic analysis, also calculated in the hydrostatic sizing (subsystem design), see Figure 1. A damage stability analysis is not done. The added mass $\mathbf{A}(\omega)$, the potential damping coefficient $\mathbf{B}(\omega)$ and the first-order wave excitation force coefficient $\mathbf{X}(\omega)$ is calculated with the panel code Ansys AQWA. The hull shape geometry is created within Ansys APDL and then exported to AQWA, see (Sandner, Yu and Cheng, Parameterized Dynamic Modelling Approach for Conceptual Dimensioning of a Floating Wind Turbine System 2015) and (Yu 2014). A routine modifies the input file for the desired wave heading angles and the wave frequencies. Depending on the element size of the surface mesh, see Figure 2, for the potential flow calculations the maximum possible wave frequency can be determined by AQWA, see (Ansys 2009). Depending on this value the range of frequencies is set. It was verified that the resulting frequency range covers all frequencies of importance for the hydrodynamic coefficients of the respective hull shape. However, a higher spatial resolution of the mesh and of the frequency resolution needs to be used for the final verification of the optimum design. For the evaluation of the different hull shape geometries of the design space first results can be extracted from this panel code calculation, see Figure 1. Especially the magnitude over frequencies of the wave excitation force coefficient or the response amplitude operator $\frac{\tilde{\xi}}{\tilde{\eta}}$, the ratio of the six rigid-body degrees of freedom $\tilde{\xi}$ and the wave elevation $\tilde{\eta}$ in the frequency domain, following the equation of motion

$$-\omega^2[\mathbf{M} + \mathbf{A}(\omega)]\tilde{\xi} + j\omega\mathbf{B}(\omega)\tilde{\xi} + \mathbf{C}\tilde{\xi} = \mathbf{X}(\omega)\tilde{\eta} = \mathbf{F}_{exc}(\omega) \quad (1)$$

can be a good indicator of the rigid-body response of the floating body to wave excitations. If the controller and the wind turbine structural dynamics are not considered the RAO can give a preliminary result for the response of the rigid body due to waves only.

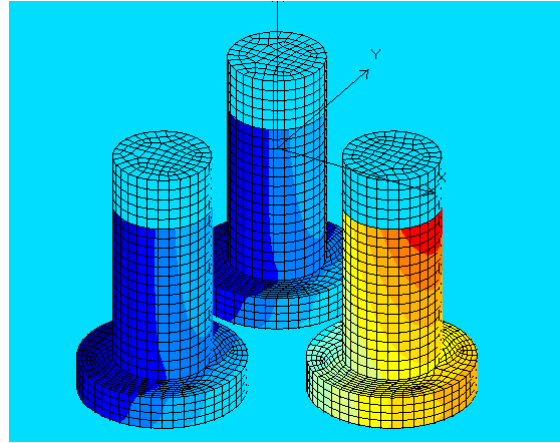


Figure 2: Ansys AQWA model showing mesh and pressure contours.

The resulting input data from the panel code to the coupled simulation model SLOW is the added mass matrix, interpolated at the respective eigenfrequency \mathbf{A}_c about the platform center of mass. The wave excitation force coefficient gives, multiplied with the wave amplitude spectrum, and followed by an inverse Fourier transform the wave excitation force timeseries. For simplicity it is assumed that the magnitude of the potential damping from the panel code is much smaller than the viscous damping (Morison damping) due to the cylindrical shape of the columns of the semi-submersible, see (Kvittem, Bachynski and Moan 2012) or (Matha, Schlipf, et al. 2011). Therefore, the potential damping is neglected in the SLOW model resulting in a higher computational efficiency because the numerical calculation of the wave radiation convolution integral is avoided. It is mentioned though, that the validity of this assumption needs to be verified in a final higher-fidelity simulation of the optimum design. Also radiation memory effects are neglected in this simplified model, which is usually of small impact for FOWT platforms.

2.2 Mooring dynamics

The differential equation for a stationary line is solved analytically. According to (J. Jonkman, Dynamics Modeling and Loads Analysis of an Offshore Floating Wind Turbine 2007) the resulting nonlinear system of equations for the horizontal displacement x_F and the vertical displacement z_F of the fairleads with the corresponding horizontal force H_F and the vertical force V_F has the form

$$\begin{aligned} x_F &= f(H_F, V_F) \\ z_F &= f(H_F, V_F). \end{aligned} \quad (2)$$

Applying a numerical solver, the forces on the fairleads can be obtained for various displacements x_F and z_F . Eventually, a function interpolates this data and returns the quasi-static external forces on the platform body during runtime. Figure 3 shows the force-displacement lookup table. Inputs to the model are the line properties and the positions of anchors and fairleads.

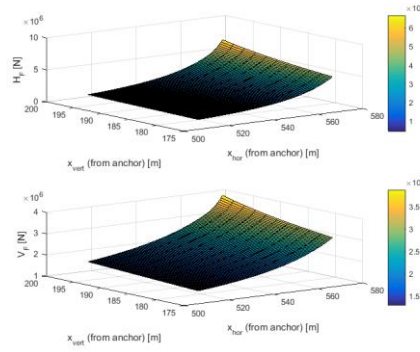


Figure 3: SLOW nonlinear quasi-static mooring forces (Lemmer, Müller, et al. 2016).

2.3 Aerodynamics

Aerodynamics are simplified by an application of the resulting thrust force of a rotor-effective wind field at hub height. In a preprocessing step BEM simulations are carried out for various tip-speed ratios λ and blade pitch angles Θ until a steady state is reached. The results are stored in two-dimensional look-up tables for the thrust c_T and torque c_P coefficients. By using the rotor effective wind speed v_0 which is a weighted average of the three-dimensional turbulent wind field on the entire rotor plane the resulting thrust and torque forces are calculated (s. a. (Lemmer, Azcona, et al. 2016)). Second, a transformation of this estimation into the rotor coordinate system is necessary, so that the relative horizontal wind speed is computed. Finally, the relative rotor effective wind speed takes the form

$$v_{rel} = v_0 - \dot{r}_{rotor,x}. \quad (3)$$

This is the scalar disturbance necessary to calculate the thrust force F_{aero}

$$F_{aero} = \frac{1}{2} \rho \pi R^2 c_T(\lambda, \Theta) v_{rel}^2 \quad (4)$$

and the external aerodynamic torque acting on the rotor body M_{aero}

$$M_{aero} = \frac{1}{2} \rho \pi R^3 \frac{c_P(\lambda, \Theta)}{\lambda} v_{rel}^2 \quad (5)$$

with air density ρ and rotor radius R . The described method has already been tested and successfully implemented for nonlinear model predictive control (NMPC) in (Schlipf, Sandner, et al. 2013) .

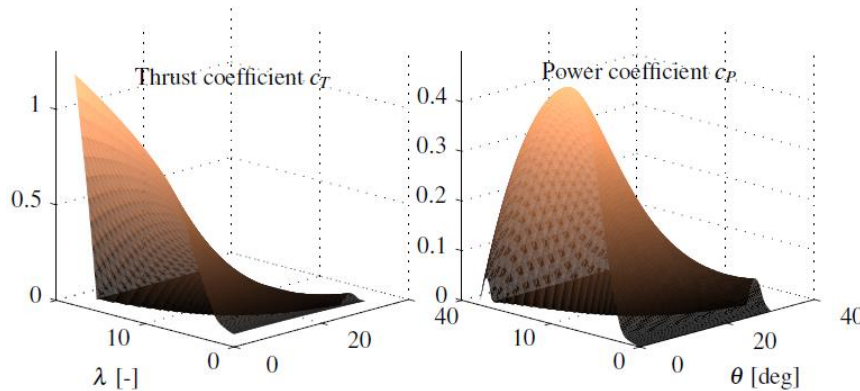


Figure 4: Example thrust and power coefficient look-up tables identified with AeroDyn (Craig and Laino n.d.).

This method neglects any dynamic effects, like dynamic inflow. The advantage is, however, that it is computationally more efficient than applying BEM theory in every time step since with this “actuator point method” no recursions and integrations over the blade span are necessary. The linearization of the aerodynamic forcing is also straightforward using the look-up tables of Figure 4. The derivation of the linearized forces and moments can be found in (Lemmer, Raach, et al. 2015).

2.4 Reduced-order simulation model SLOW

Simplified system models for FOWT have been presented in the literature. One example is the model QuLA, introduced in LIFES50+ D4.1, (Lemmer, Müller, et al. 2016), and another one can be found in (Karimirad and Moan 2012). The applications are usually a fast load case assessment or conceptual design of the system or also the controller. The range of validity has to be determined according to the selected simplifications. The coupled FOWT system is modelled in SLOW as a multibody system of rigid or flexible bodies, which are implemented as modally reduced bodies. Figure 5 shows a sketch of the exemplary mechanical model of the OC3-Hywind FOWT as defined in (J. Jonkman 2010). The equations of motion (EQM) are set up from a physical perspective following the Newton-Euler formalism. As a result, the mathematical model is available in state-space formulation as a system of symbolic ordinary differential equations (ODE), which can be directly compiled, yielding a high computational efficiency. The state vector \mathbf{x} , which consists of the vector of the degrees of freedom \mathbf{q} and its derivative $\dot{\mathbf{q}}$ is here selected as $\mathbf{q} = [x_p, z_p, \beta_p, x_t, \Omega]^T$ as platform surge, heave and pitch displacement, tower-top fore-aft displacement due to deformation and the rotor speed. This is a minimal set of DOFs which allows obtaining a good overview of the main dynamics and as a tool for controller design.

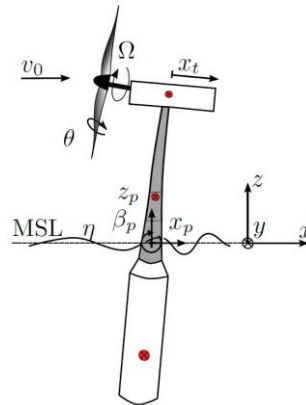


Figure 5: Topology of SLOW FOWT model showing degrees of freedom and main inputs.

The nonlinear EQM can be transformed into state space domain

$$\dot{\mathbf{x}} = \begin{bmatrix} \dot{\mathbf{q}} \\ \ddot{\mathbf{q}} \end{bmatrix} = \begin{bmatrix} \dot{\mathbf{q}} \\ \mathbf{M}^{-1}(\mathbf{p}(\mathbf{q}, \dot{\mathbf{q}}) - \mathbf{k}(\mathbf{q}, \dot{\mathbf{q}}, \ddot{\mathbf{q}})) \end{bmatrix}. \quad (6)$$

On the right hand side remains the generalized mass matrix \mathbf{M} , the generalized vector of Coriolis, centrifugal, and gyroscopic forces \mathbf{p} and the generalized vector of the applied forces \mathbf{k} . A more detailed description of the structural model can be found in (Sandner, Schlipf, et al., Reduced Nonlinear Model

of a Spar-Mounted Floating Wind Turbine 2012) and (Matha, Sandner and Schlipf, Efficient critical design load case identification for floating offshore wind turbines with a reduced nonlinear model 2014).

The symbolic equations of eqn. (6) can be linearized about an operating point \mathbf{x}_0

$$\mathbf{x} = \mathbf{x}_0 + \Delta\mathbf{x}. \quad (7)$$

With the position-dependent terms \mathbf{Q} and the velocity-dependent terms \mathbf{P} and the input matrix \mathbf{B} eqn. (6) remains as

$$\begin{bmatrix} \Delta\dot{\mathbf{x}} \\ \Delta\ddot{\mathbf{x}} \end{bmatrix} = \begin{bmatrix} \mathbf{0} & \mathbf{E} \\ \mathbf{M}^{-1}\mathbf{Q} & \mathbf{M}^{-1}\mathbf{P} \end{bmatrix} \begin{bmatrix} \Delta\mathbf{x} \\ \Delta\dot{\mathbf{x}} \end{bmatrix} + \mathbf{B}\Delta\mathbf{u}. \quad (8)$$

The aerodynamic and mooring line forces are here also represented in a linear way. See (Lemmer, Schlipf and Cheng 2016) for details. The main matrix of eqn. (8) including \mathbf{M} , \mathbf{P} and \mathbf{Q} is the system matrix \mathbf{A} . The matrices \mathbf{A} and \mathbf{B} are necessary for the derivation of the model-based controller, described in the next section.

2.5 Control

For wind speeds up to rated, a common nonlinear state-feedback law is used. This wind speed region is not critical for FOWT as it does usually not introduce a “negative damping” to the overall system as is the case for the blade-pitch control above rated conditions. The original controller of the DTU10MW reference turbine, described in (Bak, et al. 2013), is not used here because it is designed for a fixed foundation and includes a number of features which go beyond the standard implementation of a variable speed pitch-controlled turbine, like additional gains to increase the damping of certain modes in the closed loop. In order to keep things as simple as possible, the below-rated controller is designed comparably to the NREL 5MW reference wind turbine (Jonkman, Butterfield, et al. 2009). It was adapted to the DTU10MW reference wind turbine for LIFES50+ D4.1, (Lemmer, Müller, et al. 2016). Worth mentioning is the fact that, due to the blade design of the DTU10MW reference wind turbine, the generator torque does not ramp up to rated torque with a higher slope than the optimal, quadratic function of the rotor speed. It keeps a constant torque for a range of rotor speeds up to the rated speed from which the blade pitch angle increases to limit the aerodynamic torque. A description of this controller can be also found in (Lemmer, Amann, et al. 2016). For wind speeds above rated an optimal Linear Quadratic Regulator (LQR) is designed, a state-feedback controller with a diagonal feedback matrix \mathbf{K}_{lqr} , see Figure 6. The two control outputs are the blade pitch angle θ and the generator torque M_g . The states of the frequency-domain SLOW model $\mathbf{X}(\omega)$, see Figure 5, are all inputs to the controller.

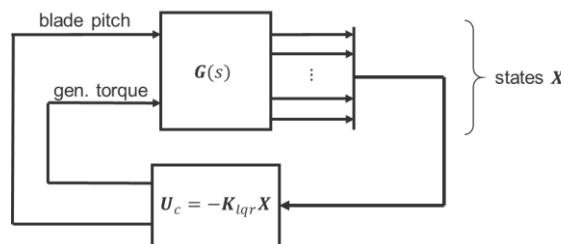


Figure 6: Linear Quadratic Regulator (LQR) block diagram.

The feedback gain matrix \mathbf{K}_{lqr} can be determined with the cost function J and the weights on states \mathbf{Q}_c and the weights on the control inputs \mathbf{u}_c , \mathbf{R}_c

$$J = \lim_{T \rightarrow \infty} \frac{1}{T} \int_0^T [\mathbf{x}^T \mathbf{Q}_c \mathbf{x} + \mathbf{u}_c^T \mathbf{R}_c \mathbf{u}_c] dt \quad (9)$$

by applying the Riccati equation, see (Skogestad and Postlethwaite 2007).

There are no sensor models and observers included in this controller but the control inputs are assumed to be perfectly measurable. This results in an optimal feedback control, which will behave as determined by the weights \mathbf{Q}_c and \mathbf{R}_c , independent of the floating platform geometry. Thus, the optimization algorithm will take the control dynamics into account but ensures that the comparison of the properties of the platform is not biased by the control. The performance of this controller and the ability to mitigate excitations from wind and waves was shown in (Lemmer, Schlipf and Cheng 2016). The weights \mathbf{Q}_c and \mathbf{R}_c used for this controller will be described in Section 3.8.

The next chapter describes the application of the previously introduced models within the optimization framework.

3 Optimization framework

This chapter focuses on the parameterization of the different simulation models and the subsystem designs introduced in Section 1.2.

Prior to the optimization, a thorough exploration of the design space is done using Design of Experiments (DoE) methods. This is necessary as an initial study to understand the main effects of the selected free variables and, if necessary, modify the initial set of free variables and their bounds. The procedure is described in more detail in the following Section 3.1. Subsequently, the evaluation of the results and the selection of a valid cost function are made.

3.1 Design of Experiments

Before applying any optimization algorithm to a given system, the overall system behaviour should be understood in order to allow adequate interpretation of the optimization results. This requires the establishment of a model approximation or a metamodel, serving as surrogate of the considered system. The optimization algorithm is then first tested on and evaluated with the metamodel before leaving the optimization algorithm to itself. A sensitivity study of the free variables yields a valid definition of the free variables and their bounds as well as a suitable cost function.

For problems involving multiple variables, simple brute force simulation-based evaluation of the system response requires large time and computational effort. In this work, for example, four input variables have been chosen. A brute force variation when considering five values for each considered variable would lead to a total amount of $5^4 = 625$ simulations that need to be evaluated. This poses a certain challenge with respect to data handling within all three levels of the simulation chain (pre-processing, processing and post-processing), especially when considering time domain simulations from floating wind turbines. Thus it is not regarded as an ideal solution for a pre-study of the system behaviour prior to optimization of the considered system.

The DoE was originally developed by Box (Box 1960) for efficient performance of physical experiments and aims at the reduction of the necessary evaluations and hence an optimization of the information output from an experimental study. More recent developments in surrogate modelling also consider more stochastic techniques for efficient space filling (Hurtado 1998), (Wang 2007). In this work, all methods aiming at efficient metamodeling are covered within the term DoE.

Application of the methodology to simulation experiments has been proposed by (Kleijnen, Sanchez, et al. 2005), and is described in (Kleijnen, Design and Analysis of Simulation Experiments 2008) (Montgomery 2013) (Siebertz, Van Bebber und Hochkirchen 2010). The specific use for optimization procedures in stochastic mechanics is described in (Wang 2007) and displayed in Figure 7. A DoE based validation of simulation models for fixed bottom offshore wind turbines considering a large variation of environmental parameters is presented in (Müller, Reiber und Cheng, Comparison of Measured and Simulated Structural Loads of an Offshore Wind Turbine at Alpha Ventus 2016). The methodology is also applied for the damage assessment of floating wind turbines in (Müller, Dazer und Cheng, Damage Assessment of Floating Wind Turbines Using Latin Hypercube Sampling, In Preparation 2017).

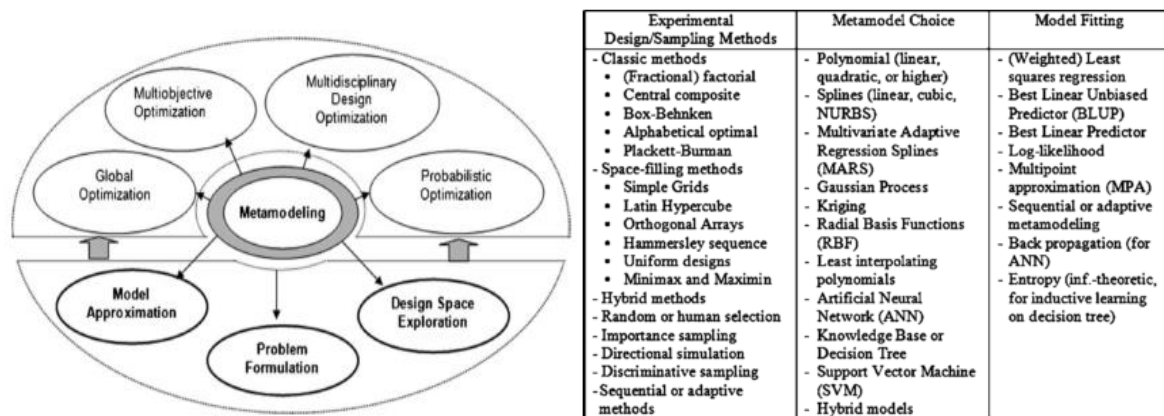


Figure 7: Metamodeling as part of system optimization (left), techniques of metamodeling (right) (Wang 2007)

In this work, latin hypercube sampling (LHS) was applied as described in (Mathworks 2016), (Siebertz, Van Bebber und Hochkirchen 2010). For this, a latin hypercube across the four dimensional design space was set up, subdividing each dimension into one hundred bins. The theory of latin hypercube design only allows each bin to be evaluated once. Within each bin, a random value is picked. An optimization algorithm as part of the sampling is essential to establish evenly distributed design points to be evaluated across the design space. Figure 8 shows an example of two possible LHS for a two dimensional problem. For the presented work, the procedure allows 100 variations of each independent parameter based on 100 simulations (in comparison: for the same resolution, a brute force computation would require $100^4 = 10^8$ simulations).

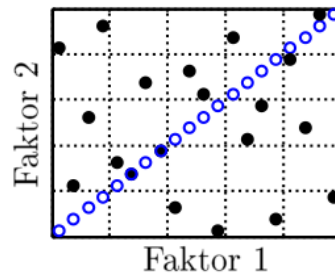


Figure 8: 2D example of a well (black) and poor (blue) distributed hypercube sampling (Siebertz, Van Bebber und Hochkirchen 2010)

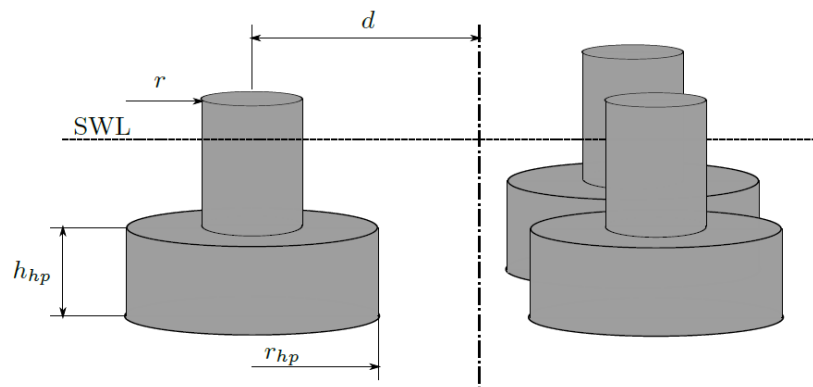


Figure 9: Hull shape optimization: Free variables

3.2 Optimization variables

The free variables or optimization variables describe the hull shape geometry of the FOWT platform, as already explained in Section 1.2. The mooring lines as well as the wind turbine remain unchanged throughout the optimization, except for the control gains. The structural design of the steel interface, as well as the control design, depends on the initial optimization variables and is done within the “subsystem design” blocks of Figure 1.

The selected hull shape parameters include the column spacing d from the platform centreline, the column radius r , the heave plate height h_{hp} and the ratio of heave plate radius r_{hp} to column radius r , \hat{r}_{hp} , see Figure 9. Table 1 shows the free variables and also the dependent variables determined by the subsystem design routines within an optimization loop.

Table 1 - FOWT design parameters.

Free variables	Dependent variables (subsystem design)
<ul style="list-style-type: none"> Platform radius r Column spacing d Heave plate height h_{hp} Heave plate radius r_{hp} 	<ul style="list-style-type: none"> Draft Steel tripod dimensions Ballast mass Platform mass distribution Mooring line fairleads position

The variables are selected with the goal of reducing the excitations from the waves for the given environmental conditions. A semi-submersible, especially with heave plates of non-negligible thickness can show a “wave-cancellation” effect where the wave forces are not transferred to the motion of the floating platform, see (Hanna 1986). It was found that the catenary mooring system does not have a major impact of the eigenmodes of the system since the stiffness's are rather small compared to the hydrostatic stiffness's in heave- and pitch-direction. The mooring stiffness in horizontal directions is of importance regarding excitations from slow-drift forces due to the small eigenfrequency resulting from the small mooring stiffness of the catenary lines and the large inertial mass of the concrete platform. This is, however, neglected in this study in order to simplify the calculations within an optimization loop. It needs to be addressed within the subsequent detailed mooring design. Depending on the fair-lead's position the mooring system can have an influence on the steady states of the FOWT, especially in pitch-direction. These effects are, however, rather small compared to the hydrostatic stiffness, which is a constraint of the optimization. Therefore, this static effect is not represented in the cost function.

3.3 Design Space

The optimization problem can cover a varying range of optimization variables. If a large range is used, linear or nonlinear constraint functions are necessary in order to discard unfeasible designs in terms of manufacturing and installation. Also, the distribution of the major system eigenfrequencies has to be verified in order to avoid a resonance due to excitation from the rotor or the waves. Such constraints are thus not known at the beginning of the optimization loop but only at the end. Only some optimization algorithms can handle these unknown constraints, like gradient-based methods, whereas others require a manual setting of the cost function to high values for such unfeasible combinations of optimization variables. For this work, it was decided to define upper and lower bounds for each of the free variables. This means that the design space is Cartesian, meaning that the range of every variable does not depend on the values of the other variables. This can be easily understood by looking at the range of heave plate radii. For small column spacing's and large column radii a design with the largest heave plate radius ratio might not be feasible. The draft, which is a result of the hydrostatic constraints, see Figure 1, is not an actual constraint of the optimization but an upper limit of ~60m was considered in the a-priori definition of the bounds of the free variables.

In order to realize such a Cartesian design space a nonlinear function of the heave plate radius ratio \hat{r}_{hp} was set up as a function of the column spacing d and the desired heave plate radius ratio $\hat{r}_{hp,in}$, see Figure 10. One can see that the derivative is equal to 1 for small x -values and deviates from a linear shape once the column spacing limits the heave plate radius for higher x -values. Other functions have been tested, e.g., “filling” the horizontal cross-sectional space between the columns by a given ratio. However, this might result in very large heave plate radii compared to the column radius, which will be unfeasible from structural design restrictions.

Table 2 - FOWT design space.

Optimization variable	Range of values
Platform radius [m]	7.0 ... 10.0
Column spacing (from centreline) [m]	18.0 ... 24.0
Heave plate height [m]	1.0 ... 10.0
Desired ratio of heave plate radius to column radius [m]	1.0 ... 2.2

A number of platform geometries from the design space are visualized in Figure 16.

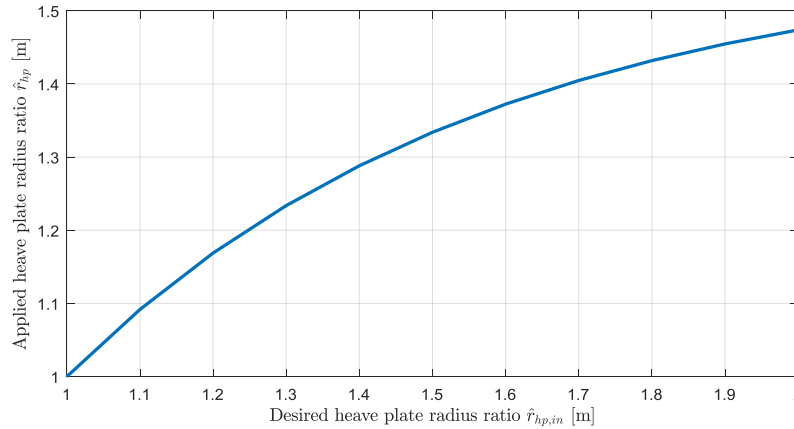


Figure 10: Nonlinear function for heave plate radius ratio r_{hp} over desired heave plate radius ratio $\hat{r}_{hp,in}$ for $d = 20\text{m}$.

3.4 Platform structural design assumptions

Depending on the free variables, first one of the free variables (draft) is determined to obtain a design which satisfies the constraint of a hydrostatic restoring in pitch of $C_{55} = 2.922 \times 10^9 \text{ Nm/rad}$ resulting in a steady-state platform pitch angle at rated wind speed of $\beta_{p, rated} = 3.5 \text{ deg}$. Second, the steel tripod on top of the concrete columns, see Figure 16 needs to be designed.

Figure 11 shows the design space satisfying the hydrostatic restoring constraint as a function of the radius on the x -axis and the column spacing on the y -axis including a constraint for the resulting draft.

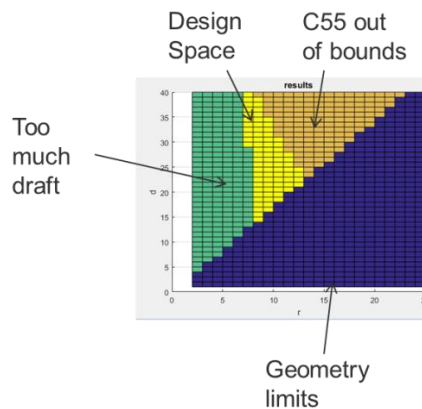


Figure 11: Hydrostatic design space exploration.

The steel tripod design is based on an approximation from public data of the Bard Tripile, supporting a 5MW wind turbine. For a parameterization of the dimensions of the steel legs (shell thickness, width, height) FEM analyses have been performed covering the presumed design space of the distance between the columns. This work was done already in the project INNWIND.EU, see (Sandner, Yu and Matha, et al. 2014) and for the design of the TripleSpar platform, see (Lemmer, Amann, et al. 2016). The Bard Tripile consists of three cylinders that are connected by square-shaped bars. While the bard

transition piece is permanently bonded to three piles by a grout connection, the TripleSpar tripod will be connected to the three concrete spars.

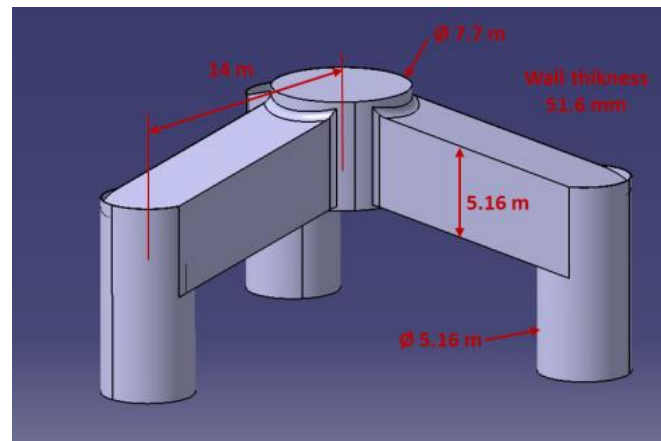


Figure 12: Dimensions of steel tripod on top of concrete columns.

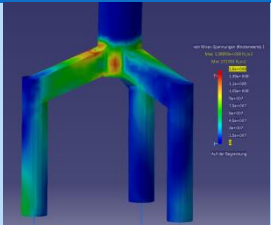
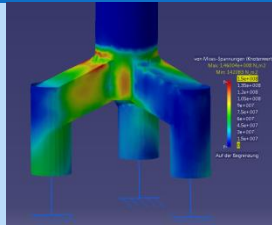
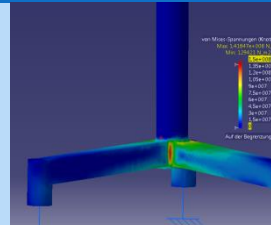
The mass of the Bard transition piece is 490 t, see (Bard Offshore 2009), which leads to a wall thickness of about 5 cm. With this geometry CATIA FEM analysis were performed to upscale the tripod for the 10MW turbine. The maximum horizontal force at the tower top of the DTU10MW turbine is 4,605

kN (Bak, et al. 2013). Because the Bard structure was designed for a 5MW turbine, the maximum force at the bard tower was assumed to be 2,303 kN, based on (Jonkman, Butterfield, et al. 2009). This

leads to a maximum stress of 139 N/mm. In the next step two tripods at distances of 10 m and 35m were designed to match this maximum stress. This is the maximum range considered for the optimization. For the other considered distances the bar height and wall thickness were interpolated.

Table 3 shows the geometry data for the bard transition piece and the smallest and the largest tripod.

Table 3 - Tripod geometry data.

	Bard Tripod	Smallest Tripod	Largest Tripod
			
Distance to centerline	10 m	10 m	35 m
Leg height	3 m	5 m	7 m
Wall thickness	0.05 m	0.05 m	0.06 m
Max hor. force	2 303 kN	4 605 kN	4 605 kN
Max stress	139 N/mm	146 N/mm	142 N/mm
Mass	490 t	447 t	1 716 t

All other design parameters can be found in Table 4. The concrete columns are assumed to be built with pre-stressed concrete following the example of the AFOSP spar design, see (Molins, et al. 2014). The wall thickness assumption is based on the same project and is not subject to a subsystem design loop here but constant for all geometries. The material cost is a lump cost for the processed material, meaning the total cost including manufacturing and assembly costs. The steel cost value is a contribution by LIFES50+ partner Olav Olsen and the concrete cost is an average of the value of the project AFOSP and the value from Olav Olsen due to the large difference between the values. It needs to be mentioned that these values are very rough indications, which can vary due to concrete shrinkage and also due to price variations over time.

The tower design is not included in this study. As mentioned earlier, the method assumes a rather small design space, which is defined based on experience and preceding spreadsheet calculations. Therefore the scatter of platform eigenfrequencies is limited. It is mentioned, however, that the tower design can be a bottleneck for wind turbines as large as 10MW. Due to the limits of the maximum tip speed the rotor speed is smaller than for turbines of smaller size. This means that the 3p frequency (blade-passing frequency), which is usually above the tower eigenfrequency, might overlap for some below-rated wind speeds with the tower eigenfrequency. Here, an exclusion-zone to be defined for the controller might be necessary but is neglected in the present work. Including the tower design in the optimization might also lead to improved designs. The freeboard is not included in the structural subsystem design for reasons of simplicity. A height of the tower base of 10m above SWL was assumed for all designs. The compliance of final design concerning the freeboard restrictions needs to be verified in the subsequent preliminary design.

Table 4 – Structural design assumptions.

Parameter	Value
Concrete column wall thickness [m]	0.4
Reinforced concrete average density [kg/m ³]	2750
Steel density [kg/m ³]	7750
Ballast density [kg/m ³]	2500
Processed steel cost [€/kg]	4.5
Processed concrete cost [€/kg]	0.399

3.5 Hydrostatics and hydrodynamics

The hydrodynamic design and evaluation of the substructure is done as an automated three-step procedure. At first a hydrostatic analysis of the platform is done in a spreadsheet design using analytical formulae and approximate ULS conditions for the thrust force. Hereby the pitch diagonal element of the hydrostatic restoring matrix (C_{55}) is fixed so that the thrust force at extreme wind conditions does not lead to an excessive platform pitch angle as described in Section 3.4. The results of the hydrostatic analysis include the hydrodynamic stiffness in pitch, heave and surge direction as well as restoring and buoyancy forces of the platform.

3.5.1 Potential flow simulations

In a second step the frequency dependent added mass and linear damping matrices of the platform are derived in the frequency domain using the panel code Ansys AQWA. For the rigid-body RAO calculation, which is a preliminary result within each optimization loop, see Figure 1, the hydrodynamic coefficients from Ansys AQWA need to be transformed from SWL to the center of mass of the FOWT using the system transformation matrix, see (Fossen 2011). The hydrodynamic properties obtained in those two preprocessing steps are then fed into the SLOW model for the time domain simulations.

The potential flow calculation is the most time-consuming simulation within the optimization (it takes between 2 and 5 Minutes on a standard PC). This is why the mesh is selected to be as coarse as possible, still covering all eigenfrequencies and the wave spectrum. The maximum allowable wave frequency for a given mesh is limited by Ansys AQWA, see (Ansys 2009). Usually, the tower eigenfrequency of $\sim 0.3\text{Hz}$ is not covered in the potential flow calculations. However, for FOWT system simulations, commonly the wave excitation frequency has an upper bound defined by the Massel number, (Massel 2001) such that no unrealistic excitations (of e.g. tower) from small surface waves of high frequency, which might also originate from numerical reasons, occur. On the other hand excitations from the tower might transfer to the platform having an impact on the radiation dynamics. This effect needs to be included in the next, preliminary, design phase using higher-fidelity models.

3.5.2 Hydrodynamic viscous damping

As mentioned before the viscous damping from flow separation is the dominant damping contribution of FOWT. It is usually well modelled through Morison equation, if the drag coefficients are calibrated well, see (Morison 1953), also in a modified manner in vertical direction for heave plates as in (Robertson, et al. 2014). However, in this work a simplified estimation is done, based on the linear damping ratios of the TripleSpar platform (Lemmer, Amann, et al. 2016). Thus, the damping ratios ξ_i in percent of critical damping are constant for all platform geometries and the linear viscous damping coefficient d_i remains as a function of the mass M_i , the added mass A_{ii} and the respective restoring stiffness C_{ii} as

$$d_i = 2\xi_i\sqrt{(M_i + A_{ii})C_{ii}}. \quad (10)$$

An improved representation of the viscous heave plate damping is part of the next developments of the framework. For the surge direction the linearized mooring stiffness has been used as C_{11} . It is noted that for simplicity equation (10) is a scalar equation neglecting the cross-coupling effects of different DOFs. The values of the assumed damping ratios for the considered DOFs can be found in Table 5. It can be seen that the value in surge-direction is larger than in heave and pitch direction. Especially, these low-frequency modes of motion will need to be re-considered for the next, conceptual design phase including dynamic mooring line models and slow-drift wave excitation forces in order to avoid resonances.

Table 5 - Hydrodynamic viscous damping ratios

Direction	Damping ratio [%]
Surge	19.22
Heave	4.8
Pitch	7.9

3.6 Mooring design

The mooring line length and the horizontal distance from the anchor to the fairleads is not varied during the optimization process. The design is based on the TripleSpar design, see (Lemmer, Amann, et al. 2016) and (M. Borg 2016). Consequently, on the fairleads radius to the centreline is varied according to the column spacing and therefore the anchor radius. This means that the platform pitch steady state under steady wind loads changes for each platform due to the different lever arm of the mooring forces on the platform. A detailed design of the mooring system for each platform, regarding fatigue loads using a dynamic mooring model needs to be done in the next, preliminary, design phase and is

out of the scope of this work. It is assumed that the impact of the mooring system on the system dynamics (eigenfrequencies and eigenmodes) is negligible, see 2.2.

3.7 Linear Model

As described in Section 2.4 the linearized SLOW model can be set up with the same input data as the nonlinear model giving the linear system description with the system matrix \mathbf{A} and the input matrix \mathbf{B} . As a prior step, the steady states of the system need to be calculated, though. This is done with the nonlinear model using a preliminary feedback controller of the wind turbine with steady wind and still sea. Based on the steady states the linear coefficients of the aerodynamic and the mooring forces are calculated. Then the symbolic equations are replaced by the numeric values yielding the system description. With this linear model it is basically possible to also calculate the response to irregular wind and wave spectra in the frequency domain with a very high computational efficiency. For this work, it was chosen, though, to keep the nonlinearities and use the time-domain model for the optimization. The linear model has been compared to the nonlinear model in (Lemmer, Schlipf and Cheng 2016).

3.8 Controller

The LQR as described in Section 2.5 is calculated based on the system steady states and the linear model of the open-loop (without control), see eqn. (10).

The scatter of the feedback gains of the state rotor speed, platform pitch velocity and tower-top velocity for different platforms is shown in Figure 13. It shows that depending on the eigendynamics the feedback gains are adjusted for each platform. The large scatter for the surge and heave gains might result from the fact that these DOFs are not of particular importance for the chosen weights \mathbf{Q}_c and \mathbf{R}_c .

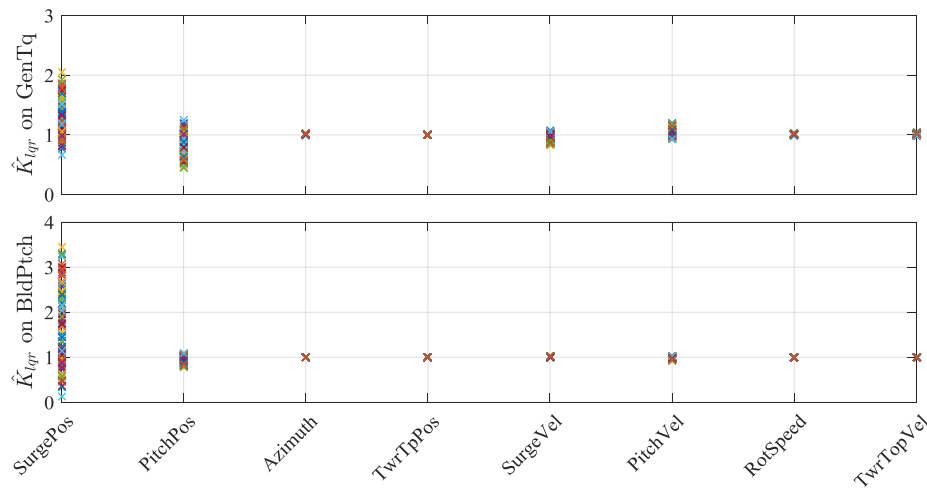


Figure 13: Scatter of the LQR feedback gains for the DoE set of platforms.

The first evaluation of the system response of all design within the bounds, see Section 4.1.1, showed that all designs were feasible in terms of hydrostatics and hydrodynamics. However, the control design method using an optimal model-based controller yields a limit-cycle behaviour for the significant wave heights above 6m, which corresponds to the wind bins of 22.1 and 25m/s, see Table 6. The reason for this is that the linearized model used for control design does not represent the nonlinearities arising from the large amplitudes at these severe operational conditions. For a dedicated control design for a given concept multiple remedies to these problems exist for the control engineer. But here, a

general automated method is necessary, valid for all of the concepts within the design space. Therefore, the selected solution is to keep the control design method but to do the optimization without the last two bins, which means neglecting a total of 0.22% of operational time at the severest conditions. It is expected that the main findings should still hold as the range of peak spectral frequencies is still wide enough to proof that the wave cancellation sought by the hull shape optimization is not an effect of a very narrow band of frequencies but holds over a range of operational conditions. Nonetheless, the issue will be part of future studies in Subtask 4.1.3.

The diagonal entries of the weight matrices \mathbf{Q}_c and \mathbf{R}_c are given as functions of the rated values (see (Bak, et al. 2013)) or maximum allowable excursions. The state weights are all zero except for the azimuth angle φ , the rotor speed Ω , the tower-top velocity \dot{x}_t and the platform pitch velocity $\dot{\beta}_p$. The weights on the states and the control inputs generator torque M_g and blade pitch angle θ are

$$\begin{aligned} Q_{c,\varphi} &= \frac{1}{(10\Omega_{rated})^2} & R_{c,M_g} &= \frac{0.4}{(M_{g,rated})^2} \\ Q_{c,\Omega} &= \frac{1}{\Omega_{rated}^2} & R_{c,\theta} &= \frac{0.001}{\left(5 \frac{\pi}{180}\right)^2} \\ Q_{c,\dot{x}_t} &= \frac{0.005}{(2\pi \cdot 0.2)^2} \\ Q_{c,\dot{\beta}_p} &= \frac{0.05}{(2\pi \cdot 0.0014)^2}. \end{aligned} \quad (11)$$

3.9 Coupled SLOW simulations

With the input files generated the time-domain simulation of the coupled nonlinear model can be started in Matlab/Simulink. Every load case runs for one hour and the initial transient is cut, although the steady states are used as initial conditions.

3.10 Load cases

As a basis for the DLCs for the SLOW simulations within the optimization the medium site of the LIFES50+ sites was used, see (Gómez Alonso, et al. 2015), p.36. As mentioned in Chapter 1 the focus is the behaviour during operation and thus, only DLC 1.2 is simulated. As said, fault conditions and extreme conditions are not covered and need to be addressed in the detailed design stage. The large excursions encountered in these DLCs exceed the range of validity of the simplified simulation models and more computationally expensive methods are necessary here. In the design basis (Gómez Alonso, et al. 2015) three different wave environments are given, here the second one is used and therefore the probability distribution of (Gómez Alonso, et al. 2015) is not used but it is assumed that the second wave environment for each wind speed holds. This results in the new probabilities according to the given Weibull distribution shown in Table 6. The peak spectral period for rated wind speeds, important for the evaluation of the wave excitation force coefficient (Section 3.1) is about 9s, see Table 6.

Each simulation runs for one hour to ensure a good resolution of the spectra and a repeatability considering the stochastic forcing.

Table 6 - Environmental conditions for DLC 1.2, extracted from D7.2 (Krieger, et al. 2015).



V_{hub} [m/s]	H_s [m]	T_p [s]	Probability
5	1.38	7	49.9%
7.1	1.67	8	21.6%
10.3	2.2	8	19.1%
13.9	3.04	9.5	7.5%
17.9	4.29	10	1.7%
22.1	6.2	12.5	0.2%
25	8.31	12	0.02%

3.11 System Optimization

This section describes the cost functions and the algorithms used for the optimization. Different sets of optimization variables and boundaries are feasible. Initially, the optimization was tested without the simulation models in the loop but using pre-determined results, to which an Artificial Neural Network (ANN) was fitted. This is described in the next section before addressing the cost function and the optimization algorithms.

3.11.1 Neural network metamodel

The metamodel used in this work for the testing of different optimization algorithms in section 7.1 was based on ANN. Due to the expected high nonlinearity of the relationships between input and output variables, five ANN fits of the LHS results were used to test different optimization algorithms. In this work, ANN with one hidden layer and $S = 5$ neurons as described in Figure 14 were applied. In the network, the R elements of the input vector p are connected to each of the S neurons in the model through a weight matrix W of size $S \times R$. Neuron specific weighted inputs (Wp) and biases (b) are collected and transferred to the output vector a .

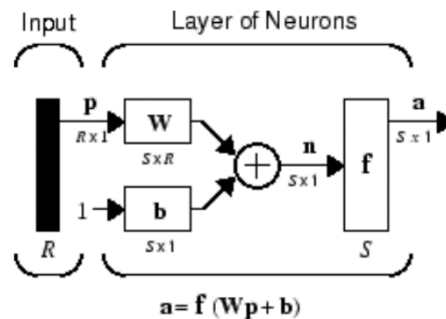


Figure 14: Setup of one-layer ANN used in this work (Hudson Beale, Hagan und Demuth 2016)

The network was trained using the Levenberg-Marquardt algorithm, which is recommended for fitting problems (Hudson Beale, Hagan und Demuth 2016). 70 % of the available results were used for training the network and another 15% for validating generalization (i.e. the attribute, that an unknown input vector close to a known one provides similar results) and to stop the training before overfitting. The final 15% were used for an independent test of the network generalization. Mean squared error was used for performance evaluation. Exemplary results indicating goodness-of-fit of the ANN describing the tower top displacement standard deviation are given in Figure 15.

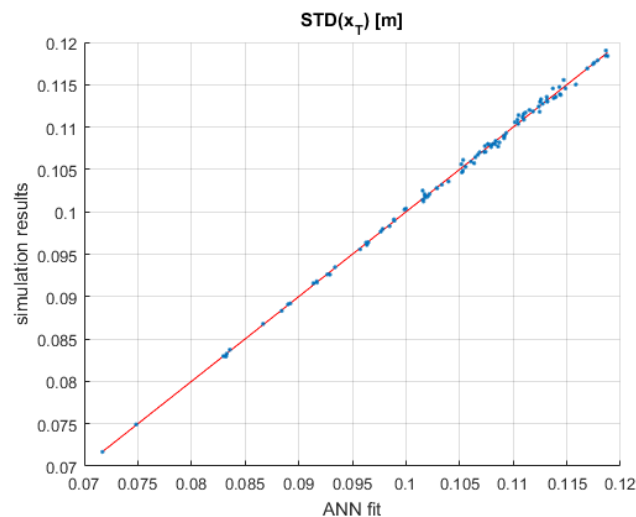


Figure 15: Performance of ANN describing standard deviation of tower top displacement.

Simulation results vs. ANN fit- results

3.11.2 Cost function

With the goal of reducing the excitations from wind and waves during operation possible outputs to be used in the cost function are the damage equivalent load (DEL) or the capital cost (CAPEX), which can be approximated from the material masses and the specific prices. The DEL resulting from a rain-flow counting gives an equivalent amplitude for a given number of load cycles. If it is weighted with the Weibull distribution for each environmental condition it gives an estimate of the fatigue loads experienced by a certain component of the system. Here, usually the tower-top displacement, relative to the tower base coordinate system is used, which is proportional to the tower-base bending moment. Other possible outputs to be included in the cost functional include the Weibull-weighted standard deviation of the rotor speed, the tower-top displacement or the platform pitch angle. The previously mentioned CAPEX of the platform in this approximation is only a rough estimate and does not include installation and transportation costs, among others, which might cover large percentages of the overall LCOE.

Different cost functionals have been tested and will be presented with the results, Chapter 4.

3.11.3 Optimization algorithms

Different optimization algorithms were tested for their suitability. The most simple and intuitive approach is a local optimum gradient based algorithm, which optimizes based on the gradient of the solution. A pattern search algorithm was also considered, as this does not require gradient information of the objective function and is hence more suitable to the optimization problem at hand. As part of the direct search optimization family, a pattern search algorithm evaluates a set of points around a given point, trying to find a more optimal solution. Finally, a particle swarm algorithm was applied, representing population based algorithms. Here, a number of particles start at different positions in the design space. Based on the evaluations of the initial points, a velocity is assigned to each particle. This way, the particles move in individual directions through the design space, updating speed and direction in each evaluation iteration. Another alternative which provided promising results was the application of hybrid methods, combining two of the abovementioned approaches. In order to provide a comprehensible procedure, this work only focused on more simple solutions that are commonly used.

The different optimizers of the Matlab Optimization Toolbox, (Mathworks 2016), were evaluated, first for a generic set of random data and then for a pre-calculated set of results using DoE samples, see Section 3.1 and ANN models representing the results of 100 sample runs covering the design space using DoE methods. A comparison of the different optimizers can be found in the Appendix, Section 7.1.

4 Results and Discussion

Careful progression of the complexity level was applied during the development of the framework. In a first step a DoE approach was made to explore the design space with a reduced set of simulations, not with a permutation of all free variables (“brute force optimization”). With the findings of the DoE the cost function could be set up and the optimization launched according to Figure 1. Consequently DoE shows the prospect here to reduce a large number of possible combinations of platform design variables, still allowing for a set of input variables that represents the whole design space and makes it possible to fit functions to the resulting response surface (Siebertz, Van Bebber und Hochkirchen 2010). Figure 16 shows a selection of designs within the defined bounds.

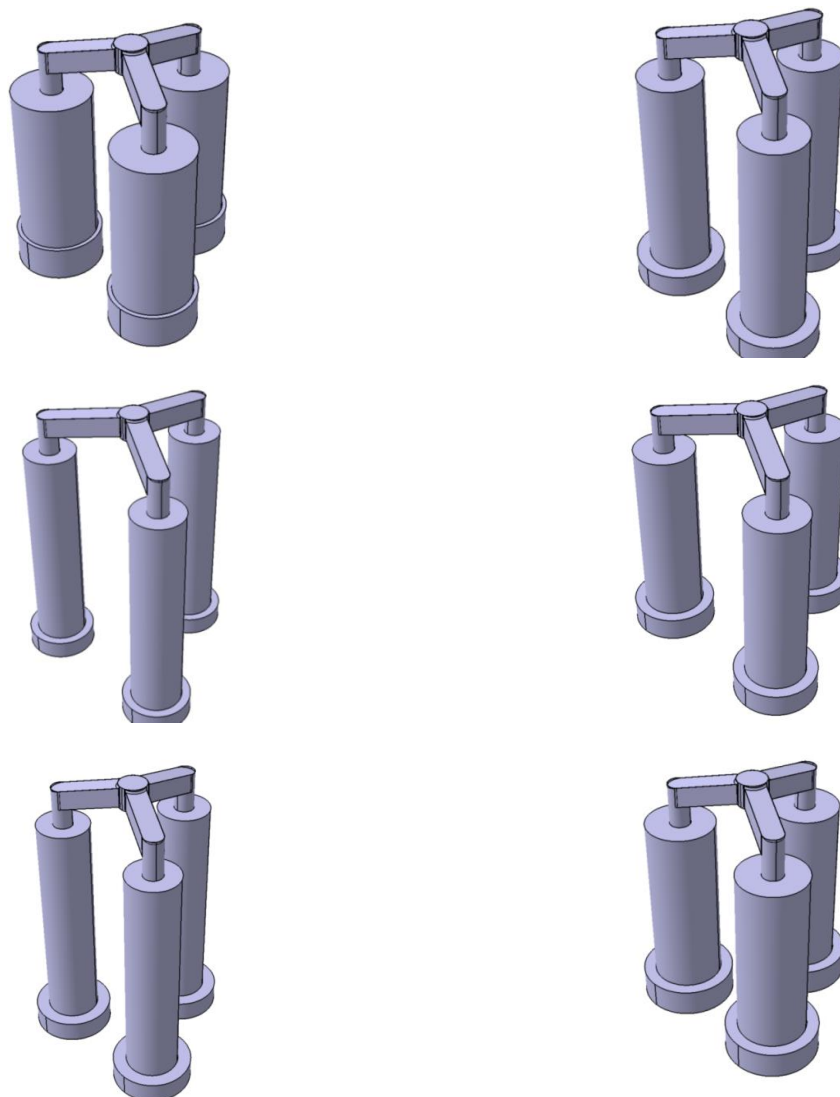


Figure 16: Selection of DoE sample geometries.

4.1.1 System response evaluation

In this section the DoE results are presented in order to identify main trends and the existence of an optimum before running a full system optimization. The found correlations can support the selection of free and cost-function variables in the design process (i.e. highly correlated parameters can be turned into dependent variables or completely neglected in order to limit the complexity of the optimization process).

Figure 17 shows a correlation analysis of the input and output variables. On the diagonal the histogram of the parameters across the results is displayed as bar plot. The even distribution across the design space resulting from the LHS can be seen (the uneven distribution of heave plate ratio results from the implemented mapping function, see Section 3.3). The Spearman correlation coefficient (Croux und Dehon 2010) is plotted as red line and given as number, indicating the relationship strength between two variables. Significant correlations (after student-t hypothesis test using $\alpha = 5\%$) are highlighted in red. The input quantities are the column radius (r), the column distance from the centreline (d), the thickness of the heave plates (hhp), the desired ratio of the heave plate radius to column radius (rhp). The selected outputs are the draft (draft), the mass moment of inertia about the horizontal y-axis (I22), the standard deviation of the tower-top displacement relative to the tower-base (Stwr), the DEL of the tower-top displacement (DEL) and the platform material cost (cost), see Section 3.4. All of the time-dependent outputs were Weibull weighted over all environmental conditions, see Section 3.10. Thus, every dot represents the calculation for a specific platform hull shape geometry with a controller designed using the linearized model. This involves a simulation with steady wind speeds for all bins and finally a one-hour simulation for each bin. The resulting dot in Figure 17 is a weighted sum over all bins. The plots on the diagonal are the histogram of the designs with respect to the parameter shown. Each scatter subplot shows combinations resulting from the LHS simulation results, which provides a general overview of trends and dependencies.

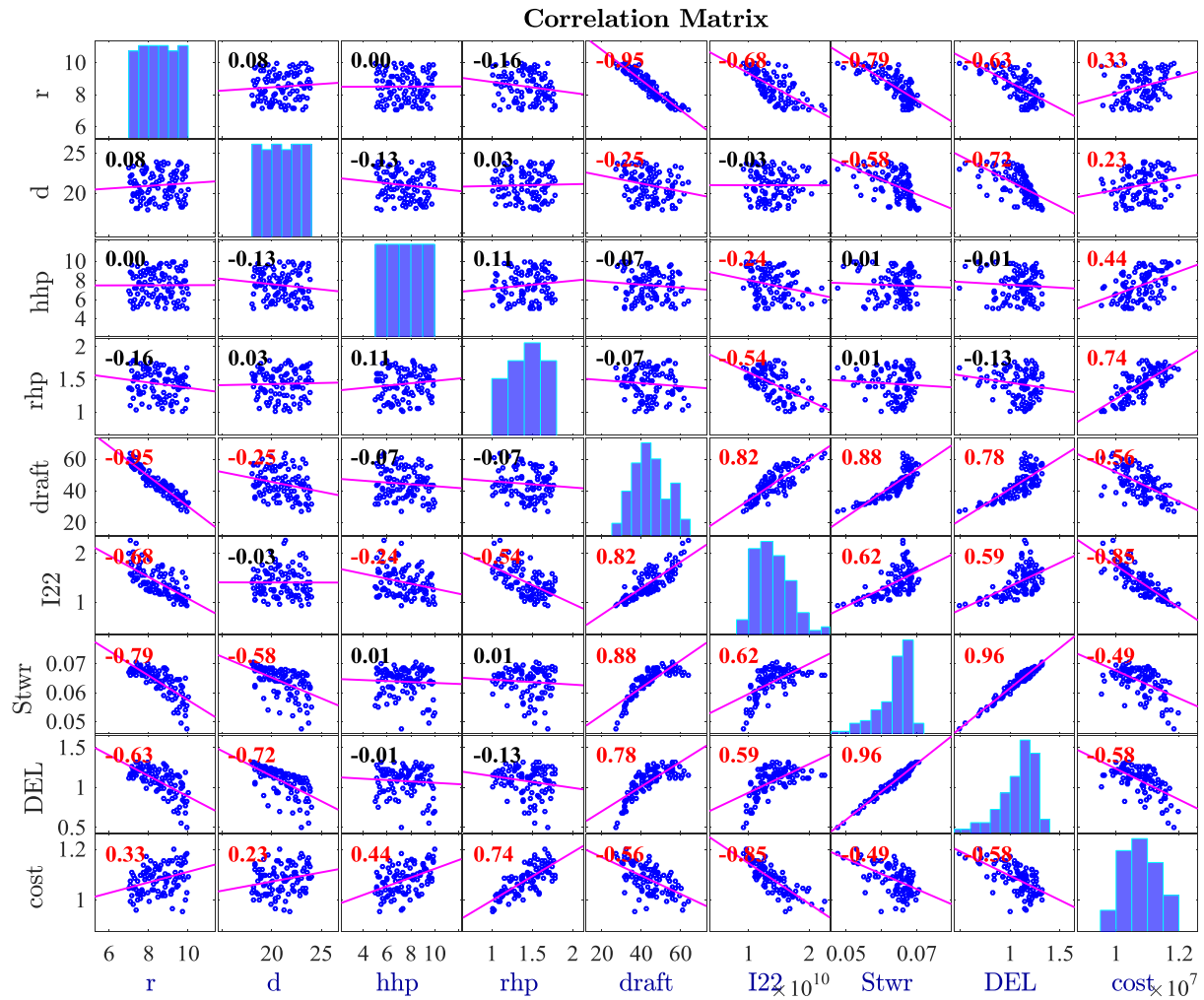


Figure 17: Correlation matrix of free variables (column radius r , distance from column to platform center d , heave plate thickness h , heave plate ratio rhp) and results (draft, mass moment of inertia I_{22} , standard deviation of tower-top displacement $Stwr$, DEL of tower-top displacement and cost of platform)

An analysis of the correlation between the free variables on the diagonal shows no significant correlation, indicating an evenly distributed base for design evaluation. On the evaluation parameter side for the system dynamic behaviour (summarized in the standard deviation and DEL of tower top displacement), and system cost a negative correlation is seen, underlining the contradicting optimization goals of a stable platform behaviour and low system costs.

The plot indicates an influence of the column radius, column spacing and the heave plate radius on the system ability to reject loads from wind and waves. The overall cost of the platform has a positive linear correlation with the platform radius, the column radius, the heave plate height and the heave plate radius due to the increased amount of material needed. The cost of the steel interface between columns and tower, which depends only on the column spacing, does not cover a prevailing portion of the overall costs.

It can be seen that the correlation between the standard deviation and the DEL of tower-top displacement, but also the standard deviation of rotor speed, electrical power and platform pitch angle is sig-

nificant ($\rho_{\text{spearman}} > 0.9$) such that it can be regarded sufficient to only consider one of the outputs to represent the magnitude of the dynamic system response to wind and waves.

Figure 18 shows the power spectral densities of the DoE set. It can be seen on top that the response to waves at $\approx 0.1\text{Hz}$ changes significantly for the different platforms, also the rotor speed, whereas the actuator action (blade pitch) is rather constant (3rd plot).

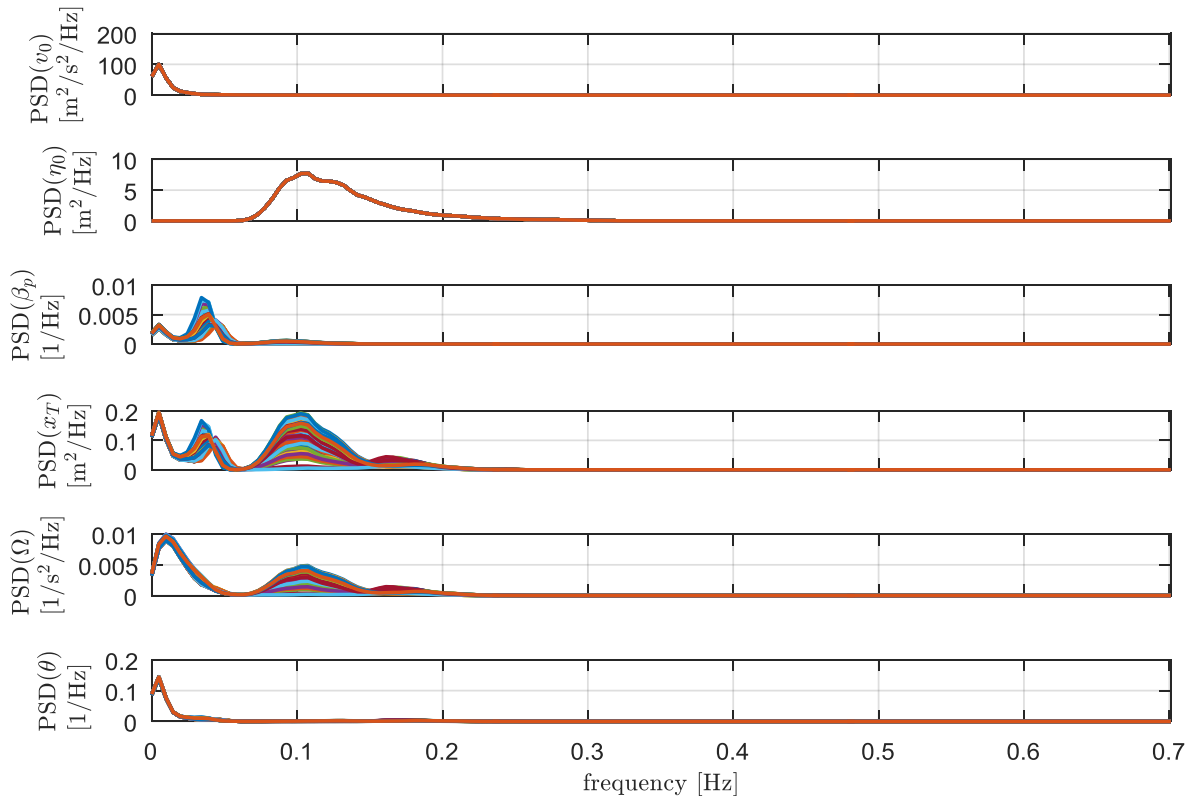


Figure 18: Power spectral densities of DoE set.

The scatter of the system eigenfrequencies over the DoE designs can be seen in Figure 19. The narrow band of scatter of each eigenfrequency allows to avoid a specific subsystem design loop checking for resonances within the optimization loop (Campbell diagram).

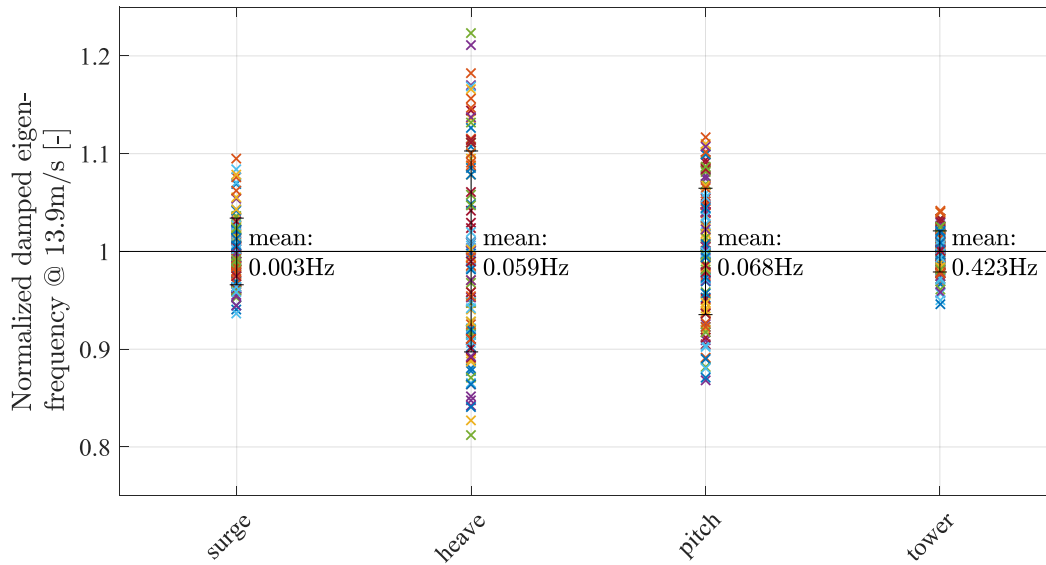


Figure 19: Scatter of system eigenfrequencies of DoE designs (open-loop, no controller).

4.2 Full system optimization

Following the design space exploration using the DoE method a full system optimization is performed according to the flow chart of Figure 1. In a first step (run #1) the cost function to be minimized by the optimization algorithm is the DEL of the tower-top displacement, Weibull-weighted over all wind bins. The objective is here to find the hull-shape with the least amplification of wind- and wave loads on the tower-top displacement. As shown in Figure 17 the tower-top displacement correlates significantly also with the rotor speed and the platform pitch angle, and thus it can be deduced that the optimum in terms of DEL is also the optimum in terms of rotor speed and platform pitch displacement.

In a next step (run #2) a cost function with weighted DEL and CAPEX according to Section 3.4 was used. The normalization of both quantities uses the results of the DoE-run with 100 example designs, described in Section 3.1

$$J = 0.61 \frac{(DEL - DEL_{DOE,max})}{DEL_{DOE,max} - DEL_{DOE,min}} + \frac{c - c_{DOE,max}}{c_{DOE,max} - c_{DOE,min}}. \quad (12)$$

The weighting of the DEL with a factor of 0.61 results from the Pearson-correlation (only linear dependencies) of the cost over DEL. It has a value of 0.58 for the Spearman correlation shown in Figure 17. For both optimizations the Pattern Search algorithm of Matlab described in Section 3.11.3 was used as it showed the best performance in the preliminary tests using interpolations and an ANN model of the DoE results, see Appendix 7.1. It was shown that it depends strongly on the selection of the initial point. Therefore, it was chosen to be as close as possible to the expected optimum (from the knowledge of the DoE, or run #1, respectively). The settings for both runs can be found in Table 7. Figure 20 shows the hull shapes and the hydrodynamic coefficients of the best performing design of run #1 (DEL only) on top and the least favourable design in terms of DEL only at the bottom. It can be seen that the heave plates at little distance below SWL lead to a significant cancellation of the wave excitation forces. This can be seen in the normalized wave excitation force coefficient $X(\omega)$ for the pitch direction (lower, center), which has a smaller magnitude, especially around the peak spectral

frequency of $f_p \approx 0.1\text{Hz}$ than the lower design. Especially the pitch direction is important for FOWT as was shown in previous works like (Lemmer, Schlipf and Cheng 2016). This fact results also from Figure 20 where both designs have a comparable RAO in surge direction.

Table 7 – Optimization settings.

	Run #1	Run #2
Optimizer	Pattern Search	Pattern Search
Cost function	$f(\text{DEL})$	$f(\text{DEL}, \text{CAPEX})$
Number of function evaluations	175	120
Function tolerance	0.01	0.01
Initial design	column radius 9.3m	column radius 10m
	column spacing 20.8m	column spacing 22.14m
	heave plate thickness 10.0	heave plate thickness 9.73
	Heave plate radius ratio 1.7	Heave plate radius ratio 1.7
Result: DEL	0.2357	0.3353
Result: CAPEX	47.1M€	9.4M€

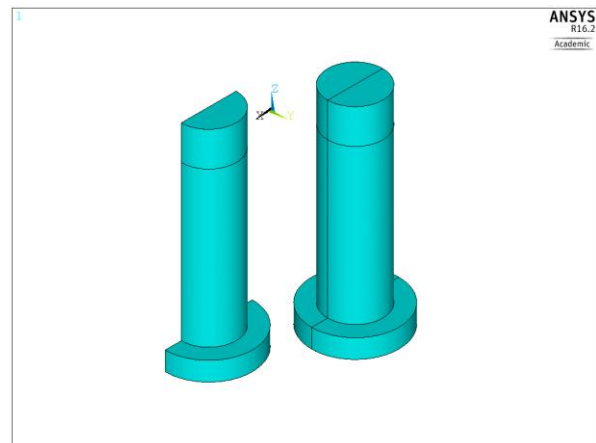
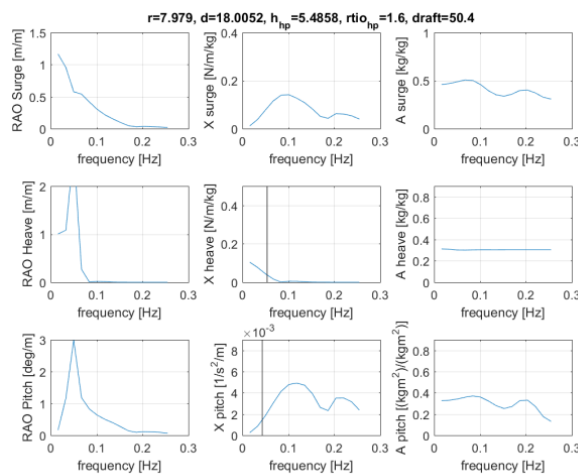
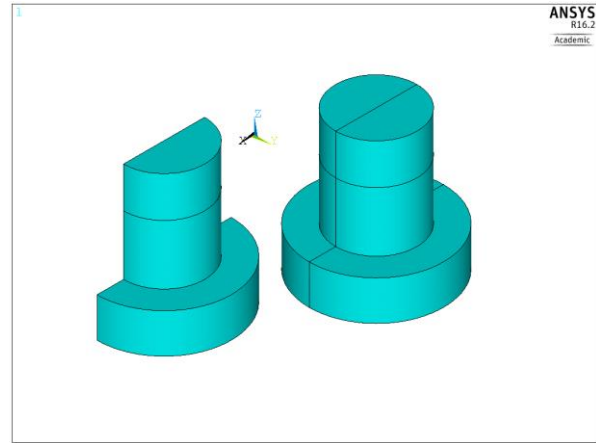
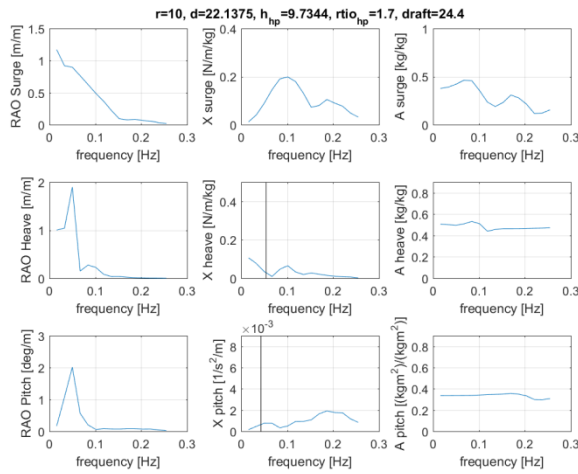


Figure 20: Optimization run #1 hydrodynamic coefficients and geometry: Best design with cost function including overall DEL only (upper row); Least favourable design of DoE with same cost function (lower row).

Figure 21 shows the hull shapes and the hydrodynamic coefficients of the best performing design of run #2 (DEL and CAPEX) on top and the least favourable design in terms of the same cost function at the bottom. It is noticeable that the heave plates do contribute significantly to the CAPEX and therefore the optimizer seeks to reduce them to a minimum, still reducing the wave excitations through an adjustment of the column spacing, the column radius and the draft (which is a function of both). The wave excitation force coefficient $X(\omega)$ shows a comparable magnitude for both platforms, although both are smaller than the lower one of Figure 20, which focuses on the DEL. It is noticeable that the draft is limited also in run #2 and therefore the optimizer does not converge towards a slender spar-type geometry. This contradicts with the common understanding that spar-type platforms feature little material costs and a well damped dynamic behaviour. This question will be analysed more in detail in the future.

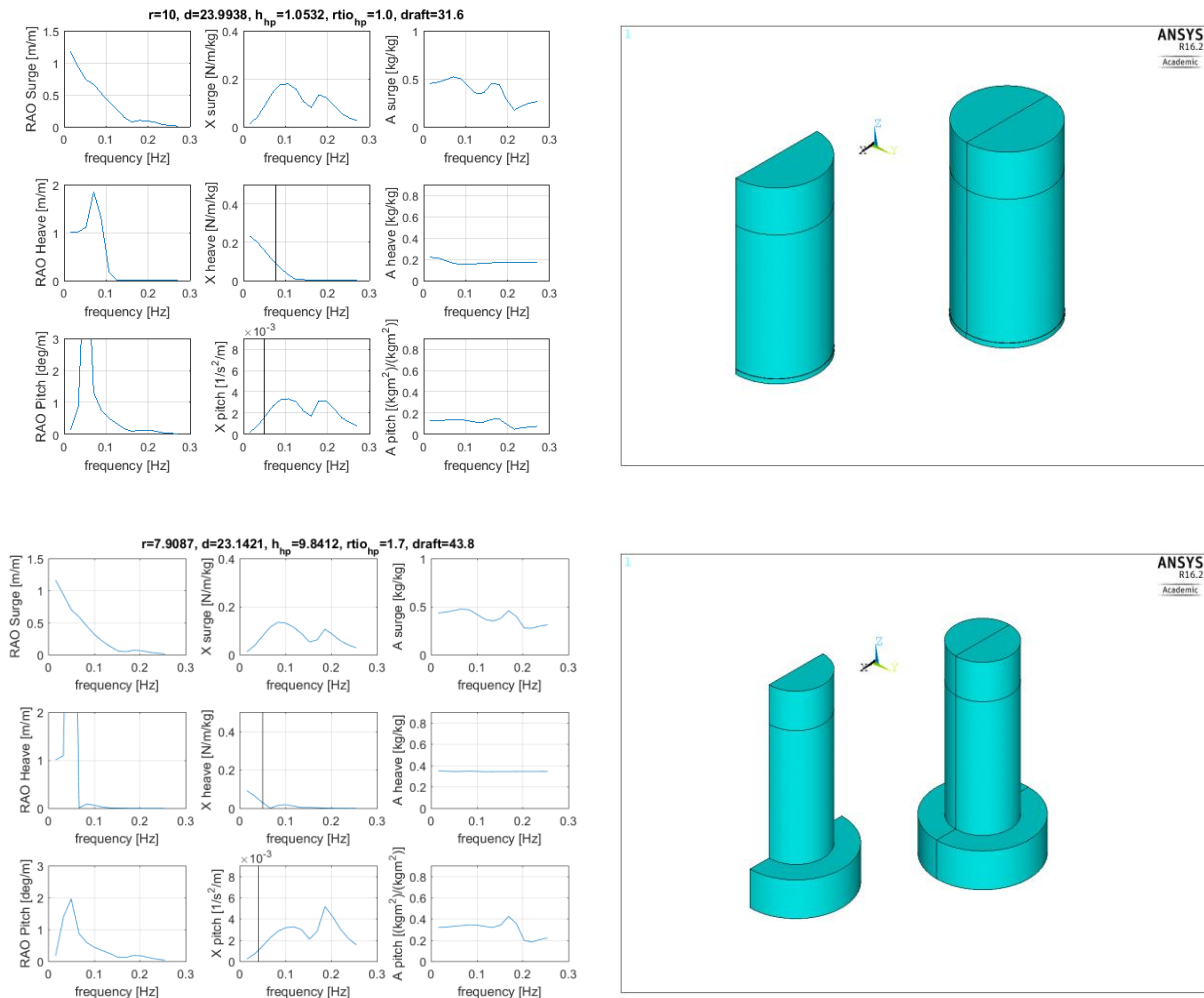


Figure 21: Optimization run #2 hydrodynamic coefficients and geometry: Best design with cost function including overall DEL and CAPEX (upper row); Least favourable design of DoE with same cost function (lower row).

In order to understand the frequency response of the resulting designs the power spectral density (PSD) was plotted for the wind speed at $v_0 = 13.9\text{m/s}$, the wave height, the tower-top displacement, the rotor speed and the platform pitch angle in Figure 22. It can be seen that the least performing design of run #1 (blue) shows the largest amplification of the wave loads $f_p = 0.1\text{Hz}$ on tower-top displacement and rotor speed. The optimum of run #2 (DEL and CAPEX) gets less excitation at the same frequency and the optimum of run #1 (DEL) features a notably reduced response. The response at low frequencies is also different but here the neglected slow drift excitation might yield differences for higher-fidelity simulations.

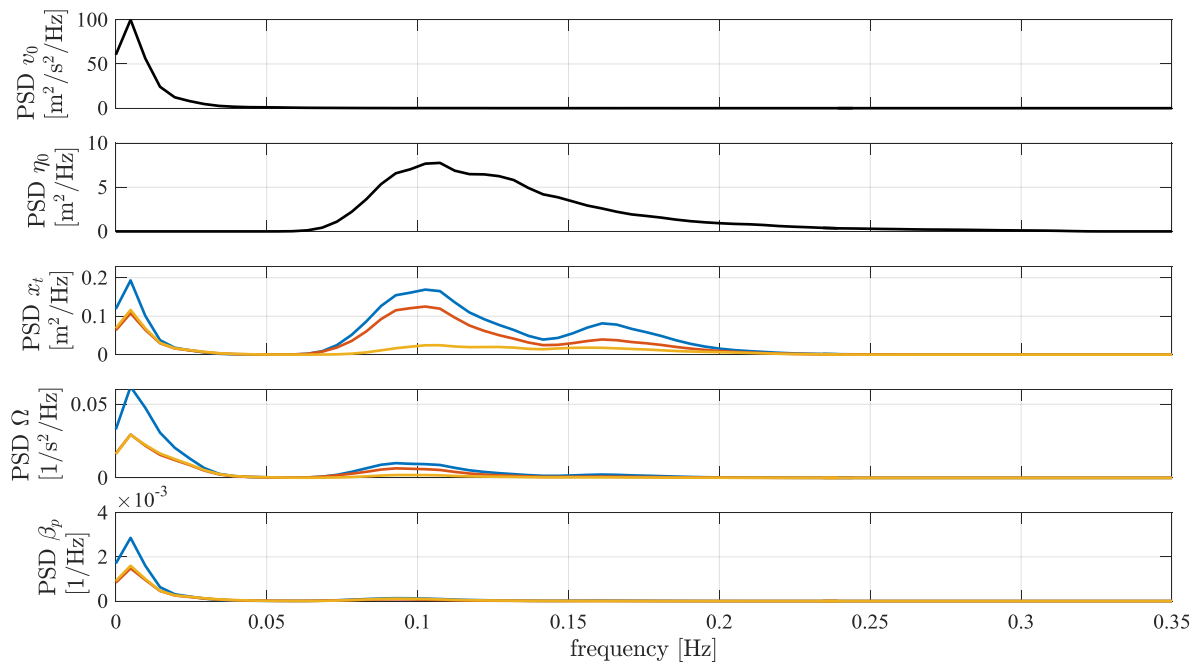


Figure 22: Power spectral densities of wind and wave height, tower-top disp, rotor speed and platform pitch angle; Least favourable DoE (blue), optimum cost, run #2 (red), optimum DEL, run #1 (yellow).

Eventually, it can be seen that the mitigation of the wave response is possible through the cancellation of the wave excitation force coefficient by optimizing the hull shape. However, this happens at a significant increase of material cost, as shown in Table 7. The material cost is more than 4 times larger for the best design in terms of tower-top displacement DEL. This increase of structural mass, however, does not seem to be the cause for the reduction of DEL, since the mass moment of inertia in pitch-direction, which is here the critical direction, see Figure 17 (I22), does not increase for an increasing cost. This means that for the designs with a high mass the draft is low and therefore close to the center of mass yielding a reduced mass moment of inertia.

5 Conclusion

The report presented a framework for the optimization of FOWT systems using simplified simulation models focusing at the reduction of excitations from environmental forcing during operation. Especially new is the inclusion of the wind turbine controller into the optimization loop where a linear model is included for control design and a nonlinear model for the calculation of the time domain response. It could be shown that with the given set of free variables of a concrete semi-submersible platform it is possible to significantly reduce the response amplitude for the given site. However, this happens at the cost of increased expenditures for the material due to an increased structural mass. The benefit is not the increased mass, but the reduced draft which requires an increased column radius to fulfil the hydrostatic restoring requirement in pitch direction. With such a low-draft semi-submersible with thick heave plates a design for wave cancellation is possible with a significant reduction of the response of e.g. the tower-top and the rotor speed to waves.

The methodology involves a design space exploration using Design of Experiments for a reduced number of load calculations. This initial study reveals the sensitivities of different geometric parameters and allows for a reasonable setup of the control problem: a valid design space of feasible concepts, a meaningful selection of the free variables and a cost function yielding a result which fulfils the previously determined requirements.

Different single-objective optimization algorithms, like the Genetic Algorithm, a Particle Swarm Optimizer and the Pattern Search Method were assessed using generic datasets but also the results from the design space exploration. The response surface was evaluated once through four-dimensional interpolation but also through an Artificial Neural Network. This analysis gives important findings on the sensitivity of the result and the number of necessary iterations with respect to the optimization algorithm and also the initial point.

Finally, two optima were presented, one for a single objective of reducing the Damage Equivalent Load of the tower and one also including the material cost. The power spectral density of the different optima shows a significantly better response compared to the least favourable design of the design space exploration study, also if the material cost is considered. The presented methodology is, in general, applicable in the same way to steel platforms and to other types of floating wind turbine platforms.

6 Outlook

In a next step in LIFES50+ the optimization framework will be applied to optimize the two generic concepts to be selected in D4.2. While the general findings are considered valid, a higher-fidelity study in the subsequent design phases, including other load cases and ultimate loads, is necessary to prove the results and to proceed with the detailed subsystem design (e.g. detailed structural design, mooring design, etc.). Regarding the system dynamics aerodynamic models with Blade-Element-Momentum Theory and the necessary correction models including dynamic inflow including flexible blades should be used at least to verify the aerodynamic damping including control. Including side-side dynamics and wind/wave misalignments will make the control design process more realistic accounting for resonances or bandwidth limitations of the actuators. On the hydrodynamics side a higher-fidelity simulation will include finer meshes and a verification of the hydrodynamic damping through model tests and the inclusion of second order forcing will allow a verification of the mooring design.



Future studies aiming at Multidisciplinary Design and Optimization will include a more complex cost function: Then the objective is not to find how the dynamic response can be reduced but an optimal solution is sought in terms of systems engineering. This includes the selection of the most suitable platform type for a given type including e.g. transportation, installation and Operation and Maintenance. The base material concrete used here might not yield a sustainable solution for FOWT due to the limited availability of sand as a natural resource. In turn, the increased lifetime should be taken into account for in the cost model. In WP 7 of LIFES50+ design guidelines and standards are developed. It will be studied how the findings of the presented study can be included in a recommended design practice. It will be essential to find out whether the inclusion of the wind turbine controller alters significantly the results compared to using linear frequency-domain methods (panel code) of a rigid body, only.

7 Appendix

7.1 Evaluation of optimization algorithms

The optimization problem in this work contains multiple local optimum, thus Matlab Global Optimization Toolbox is used for the optimization, which has five global optimization solvers, i.e multistart, pattern search, genetic algorithm, global search, and simulated annealing.

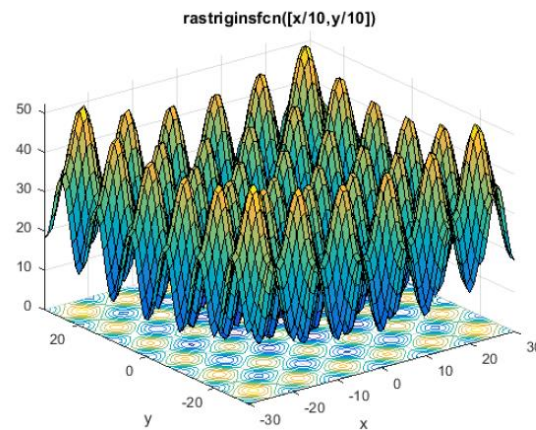


Figure 23: Plot of Rastrigin's function

In (Mathworks 2016) example is presented, which shows how to minimize Rastrigin's function (shown in Figure 23) with five solvers. The characteristics of each solver lead to different solutions and run times. The results, examined in the table below shows the difference between these five solvers, where objective is the minimum which is found by the solver, "#Fevals" represents the function evaluations.

Table 8 – Generic comparison of Matlab optimizers

Results	fminunc	patternsearch	ga	particleswarm	GlobalSearch
solution	[19.9 29.9]	[19.9 -9.9]	[0 0]	[0 0]	[0 0]
objective	12.9	5	0	0	0
# Fevals	15	174	5400	2300	2178

- **fminunc** quickly reaches the local solution within its starting basin, but does not explore outside this basin at all.
- **patternsearch** takes more function evaluations than **fminunc**, and searches through several basins, arriving at a better solution than **fminunc**.
- **ga** takes many more function evaluations than **patternsearch**. By chance it arrived at a better solution. In this case, **ga** found a point near the global optimum. **ga** is stochastic, so its results change with every run. **ga** has simple calling syntax, but there are extra steps to have an initial population near [20,30].

- **particleswarm** takes fewer function evaluations than **ga**, but more than **patternsearch**. Although in this case, **particleswarm** found the global optimum, but it is still stochastic, so its results change with every run.
- **GlobalSearch** run takes the same order of magnitude of function evaluations as **ga** and **particleswarm**, searches many basins, and arrives at a good solution. In this case, **GlobalSearch** found the global optimum. Setting up **GlobalSearch** is more involved than setting up the other solvers.

As is shown, although **ga**, **particleswarm** and **GlobalSearch** have found better optimums, the number of function evaluations is however much greater. Considering of the case in this report, each function evaluation includes modelling in Ansys Mechanical, hydrodynamic simulation with Ansys AQWA, controller design, time domain simulation of the whole floating wind turbine system et cetera, which takes a lot of time. In order to find a relative optimum design with less time investment, **fminunc** and **ga** are out of consideration. On the other hand, **GlobalSearch** is gradient-based, which is suitable for smooth objective function (smooth means the objective function is twice differentiable). So optimization solver **patternsearch** and **particleswarm** are further investigated.

The solver investigation work is based on the result of the design space exploration, which has four free variables and six cost function variables. Detailed information of the design space exploration is presented previously.

Presettings for both of the optimization solvers are:

- Same lower bounds and upper bounds, which is also used for the design space exploration
- Same tolerance (0.001), which means Iterations stop if the change in function value is less than the tolerance
- Same maximum number of iterations

To evaluate the solvers, two aspects are examined, one is the accuracy, and the other is the efficiency.

7.1.1 Accuracy

Accuracy here means how close is the optimum which is found by the solver to the real global optimum. The plots in Figure 24 and Figure 25 show the found optimum values and positions in both 2D- and 3D- plot. The algorithm of the cost function in the upper row is a neural network based on the database of the design space exploration. In the lower row is an n-dimension interpolation of the same data bank. “Repeat times” in the figure represents the optimized reprocessing with the same options that define the parameters of the solver. The reason is to check whether the result is robust or not. As we can see, in the case of n-dimension interpolation, particle swarm finds different optimums when optimize processing is repeated, this can be clearly discovered in the plot of optimum positions. But in general, the result with both solvers are similar, it’s difficult to tell, which solver is more accurate.

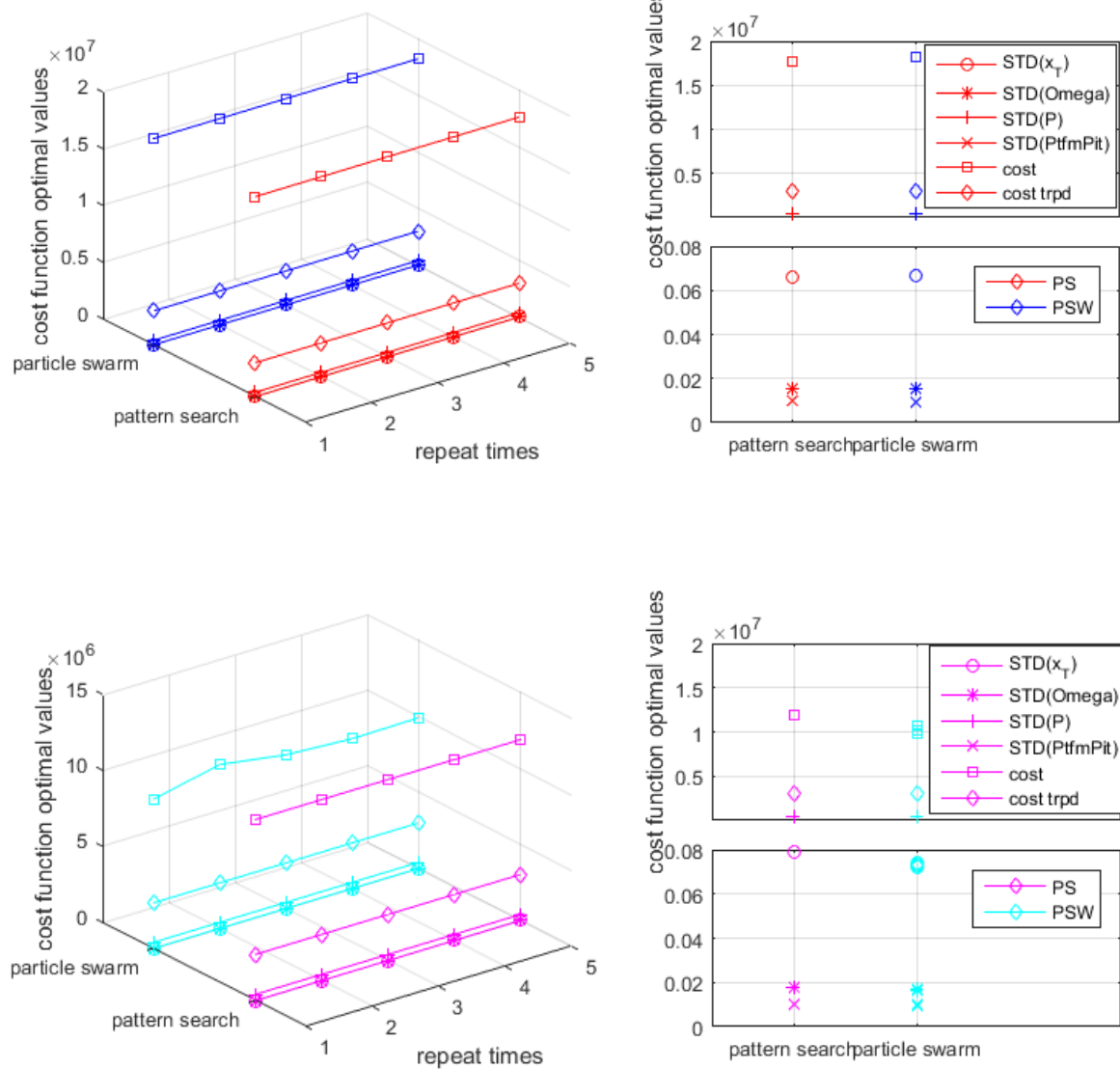


Figure 24 - Comparison of cost function optimal values with different optimization solvers.

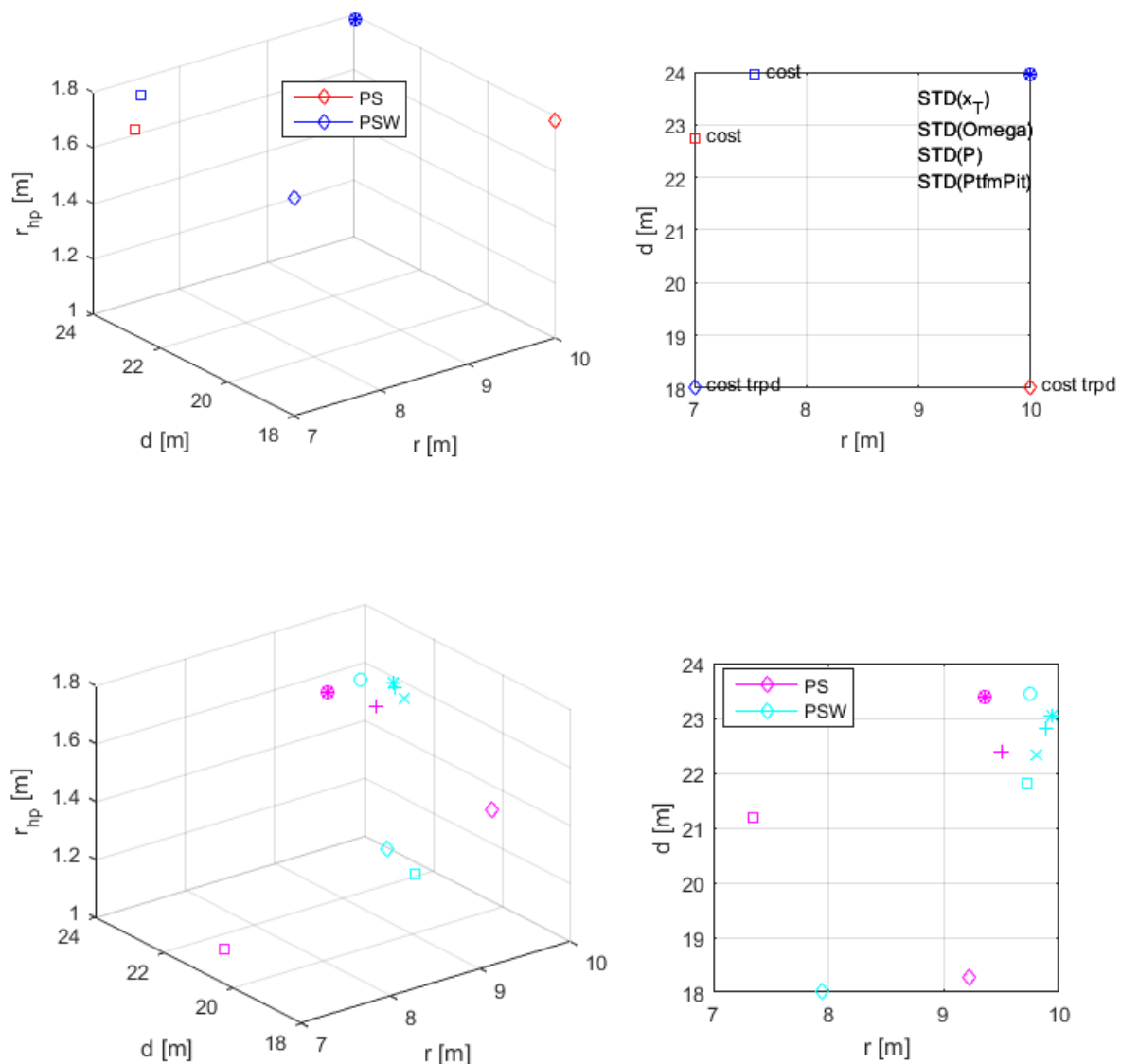


Figure 25 - Comparison of optimal positions with different optimization solvers.

7.1.2 Efficiency

As is shown previously, the difference of accuracy between the solvers is not remarkable. However, in consideration of the number of function evaluations, there is a large difference. Since each function evaluation takes a considerable amount of time. Efficiency in this optimization problem means to find the optimum with the smallest number of function evaluations. On the whole, pattern search needs less function evaluations. Important to point out, that the number of function evaluation which particle swarm needs is sensitive to the cost function. But pattern search depends more on the initial point, at which optimum search work begins, this will be discussed later.

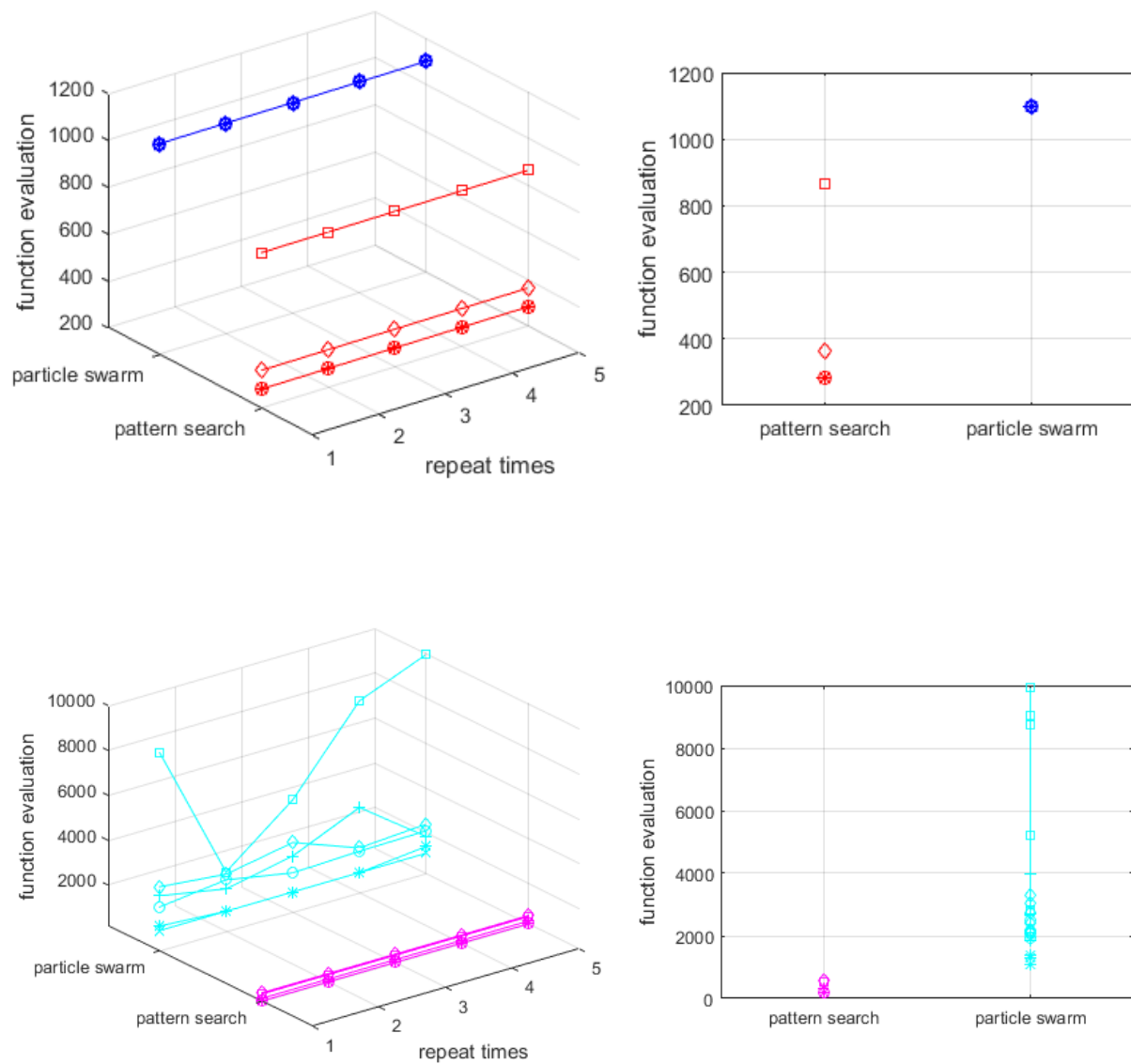


Figure 26 - Comparison of total number of function evaluations with different optimization solvers.

In consideration of the simple algorithm, smaller function evaluations and also the robust results, it is recommended to use pattern search as the optimization solver to be integrated into the dynamic simulations. The sensitivity is further studied for a more efficient implementation. Figure 27 shows the influence which comes from the initial points.

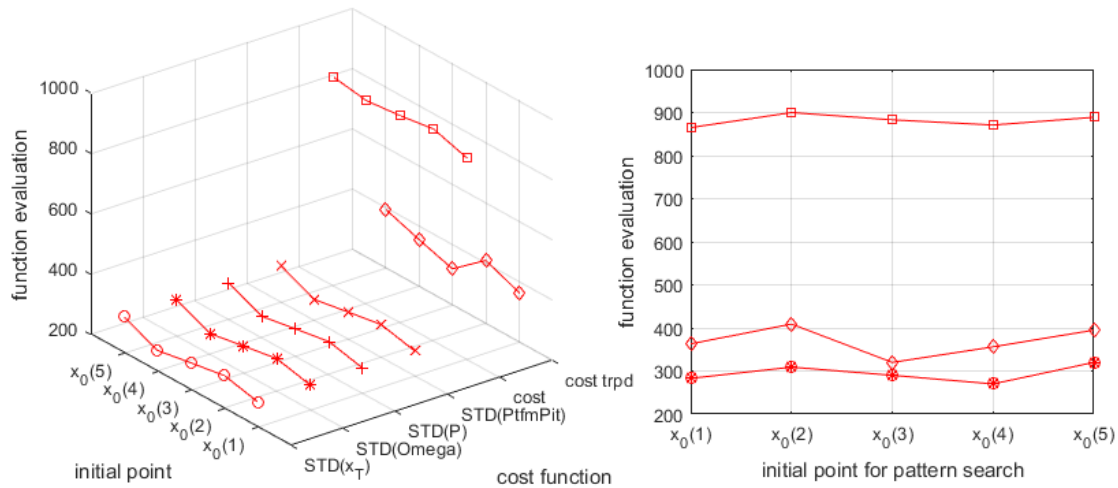


Figure 27 - Comparison of total number of function evaluations with different initial points for pattern search.

As is shown, the number of function evaluations of pattern search depends strongly on the initial point. Five different initial points are defined here, i.e. $x_0(1) \dots x_0(5)$, the number of function evaluations differs from initial point to initial point. On the other hand, a great difference is discovered between different cost objective, variable "cost" needs much more function evaluations to find the optimum. This isn't because of the difference between the cost function algorithms, but due to the fact that the exact value of "cost" is much greater than the others (which can also be seen in Figure 24). Although the tolerance for "cost" is also 0.001, which is the same as the other objective costs like "STD (x_t)", "STD (Ω)" etc., however, in consideration of the great exact value, the relative tolerance is much smaller. Thus, it is recommended that all the objective costs should be normalized.

8 Bibliography

Ansys. 2009. "Aqwa™-line manual." Tech. rep.

Aubault, Alexia, Christian Cermelli, and Dominique Roddier. 2007. "Parametric Optimization of a Semi-Submersible Platform With Heave Plates." *Volume 1: Offshore Technology; Special Symposium on Ocean Measurements and Their Influence on Design*. Asme. 471-478. <http://proceedings.asmedigitalcollection.asme.org/proceeding.aspx?articleid=1593019>.

Bachynski, Erin. 2014. "Design and Dynamic Analysis of Tension Leg Platform Wind Turbines." Ph.D. dissertation, NTNU. <http://www.diva-portal.org/smash/get/diva2:703359/FULLTEXT01.pdf>.

Bak, Christian, Frederik Zahle, Robert Bitsche, Taesong Kim, Anders Yde, Lars Henriksen, Anand Natarajan, and Martin Hansen. 2013. "Description of the DTU 10 MW Reference Wind Turbine." Tech. rep., DTU Wind Energy.

Bard Offshore. 2009. Accessed 06 2015. http://www.bard-offshore.de/uploads/tx_barddocuments/FactSheetBARD5.pdf.

Birk, Lothar, Günther F Clauss, and June Y Lee. 2004. "Practical Application Of Global Optimization To The Design Of Offshore Structures." *Proceedings of OMAE04 23rd International Conference on Offshore Mechanics and Arctic Engineering*.

Borg, M., and H. Bredmose. 2015. "LIFES50+ D1.2 Wind turbine models for the design." Tech. rep., DTU. <http://lifes50plus.eu/wp-content/uploads/2015/12/D1.2.pdf>.

Borg, M., and H. Bredmose. 2015. "LIFES50+ D4.4 Overview of the numerical models used in the consortium and their qualification." Tech. rep., DTU.

Borg, Michael. 2016. "Mooring system analysis and recommendations for the INNWIND Triple Spar concept." DTU Wind Energy Report-I-0448, Technical University of Denmark, Lyngby, Denmark.

Box, Behnken. 1960. "Some New Three Level Designs for the Study of Quantitative Variables." *Technometrics*.

Brommundt, Matthias, Ludwig Krause, Karl Merz, and Michael Muskulus. 2012. "Mooring System Optimization for Floating Wind Turbines using Frequency Domain Analysis." *Energy Procedia* 24 (January): 289-296. <http://linkinghub.elsevier.com/retrieve/pii/S1876610212011514>.

Chew, Kok-hon, Kang Tai, and Michael Muskulus. 2015. "Optimization of Offshore Wind Turbine Support Structures Using Analytical Gradient-Based Method." *EERA Deepwind*. Trondheim/NO. http://www.sintef.no/Projectweb/Deepwind_2015/Presentations/.

Craig, Hansen, and David J. Laino. n.d. "User's Guide to the Wind Turbine Aerodynamics Computer Software AeroDyn." Tech. rep.

Croux, and Dehon. 2010. "Influence functions of the Spearman and Kendall." *Statistical Methods & Applications*.



- Fischer, Boris, and Peter Loepelmann. 2016. "Balancing rotor speed regulation and drive train loads of floating wind turbines." *Journal of Physics: Conference Series* 753: 052016. doi:10.1088/1742-6596/753/5/052016.
- Fleming, Paul, Antoine Peiffer, and David Schlipf. 2016. "Wind Turbine Controller To Mitigate Structural Loads On A Floating Wind Turbine Platform." *Proceedings of the ASME 35th International Conference on Ocean, Offshore and Arctic Engineering*. Busan/Korea.
- Fossen, Thor. 2011. *Handbook of Marine Craft Hydrodynamics and Motion Control*. Vol. First Edit. John Wiley & Sons.
- Fylling, Ivar, and Petter Andreas Berthelsen. 2011. "WINDOPT- An optimization tool for floating support structures for deep water wind turbines." *Proceedings of ASME International Conference on Ocean, Offshore and Arctic Engineering OMAE*. doi:10.1115/OMAE2011-49985.
- Gómez Alonso, Pablo, Gustavo Sánchez, Alberto Llana, and Gonzalo Gonzales. 2015. "LIFES50+ D1.1 Oceanographic and meteorological conditions for the design." Tech. rep., Iberdrola. http://lifes50plus.eu/wp-content/uploads/2015/12/GA_640741_LIFES50-_D1.1.pdf.
- Hall, Matthew, Brad Buckham, and Curran Crawford. 2013. "Evolving Offshore Wind : A Genetic Algorithm-Based Support Structure Optimization Framework for Floating Wind Turbines." *OCEANS 2013 MTS/IEEE Conference Proceedings*.
- Hanna, S. Y. 1986. "Wave Cancellation Effects and Extreme Wave Dynamics." *Offshore Technology Conference*. Houston, TX/USA.
- Hudson Beale, Mark, Martin T. Hagan, and Howard B. Demuth. 2016. *Neural Network Toolbox, User's Guide*. MathWorks.
- Hurtado, Barbat. 1998. "Monte Carlo Techniques In Computational Stochastic Mechanics." *Archives of Computational Methods in Engineering*.
- Häfele, Jan, and Raimund Rolfes. 2016. "Approaching the ideal design of jacket substructures for offshore wind turbines with a Particle Swarm Optimization algorithm." *Proceedings of the Twenty-sixth (2016) International Ocean and Polar Engineering Conference (ISOPE)*. 156-163.
- Härer, Arne, Denis Matha, Daniel Kucher, and Frank Sandner. 2013. "Optimization of offshore wind turbine components in multi-body simulations for cost and load reduction." *Proceedings of the EWEA Offshore*. Frankfurt.
- Jonkman, J. 2010. *Definition of the Floating System for Phase IV of OC3*. Tech. rep., NREL.
- Jonkman, Jason. 2007. "Dynamics Modeling and Loads Analysis of an Offshore Floating Wind Turbine." Ph.D. dissertation.
- . 2008. "Influence of Control on the Pitch Damping of a Floating Wind Turbine." *Proceedings of the ASME Wind Energy Symposium*. Re, n.
- Jonkman, Jason, and Marshall Buhl. 2005. "Fast User's Guide."

- Jonkman, Jason, S Butterfield, W Musial, and G Scott. 2009. "Definition of a 5-MW Reference Wind Turbine for Offshore System Development." NREL, Boulder/USA.
- Karimirad, Madjid, and Torgeir Moan. 2012. "A Simplified Method for Coupled Analysis of Floating Offshore Wind Turbines." *Journal of Marine Structures*.
- Kleijnen. 2008. *Design and Analysis of Simulation Experiments*.
- Kleijnen, Sanchez, Lucas, and Cioppa. 2005. "State-of-the-Art Review: A User's Guide to the Brave New World of Designing Simulation Experiments." *INFORMS Journal on Computing*.
- Krieger, Antonia, Gireesh Ramachandran, Luca Vita, Pablo, Berque, Joannès Gómez Alonso, and Goren Aguirre. 2015. "LIFES50+ D7.2: Design Basis." DNV-GL.
- Kurz, Thomas. 2013. "Symbolic Modeling and Optimization of Elastic Multibody Systems." Ph.D. dissertation.
- Kvittem, Marit, Erin Bachynski, and Torgeir Moan. 2012. "Effects of Hydrodynamic Modelling in Fully Coupled Simulations of a Semi-submersible Wind Turbine." *Energy Procedia* 24: 351-362. doi:10.1016/j.egypro.2012.06.118.
- Kühn, Martin. 2003. "Dynamics and Design Optimization of Offshore Wind Energy Conversion Systems." Ph.D. dissertation, TU Delft.
- Lemmer, F, D. Schlipf, and P.W. Cheng. 2016. "Control design methods for floating wind turbines for optimal disturbance rejection." *The Science of Making Torque from Wind*. München.
- Lemmer, F., K. Müller, A. Pegalajar-Jurado, M. Borg, and H. Bredmose. 2016. "LIFES50+ D4.1 Simple numerical models for upscaled design."
- Lemmer, F., S. Raach, D. Schlipf, and P. W. Cheng. 2015. "Prospects of linear model predictive control on a 10MW floating wind turbine." *Proceedings of the International Conference on Offshore Mechanics and Arctic Engineering - OMAE*. doi:10.1115/OMAE2015-42267.
- Lemmer, Frank, Florian Amann, Steffen Raach, and David Schlipf. 2016. "Definition of the SWE-TripleSpar Floating Platform for the DTU 10MW Reference Wind Turbine." Tech. rep., University of Stuttgart. <http://www.ifb.uni-stuttgart.de/windenergie/downloads>.
- Lemmer, Frank, José Azcona, Florian Amann, and Feike Savenije. 2016. "INNWIND.EU D4.37 Design Solutions for 10MW Floating Offshore Wind Turbines." INNWIND.EU.
- Lindeberg, Eivind. 2009. "Optimal Control of Floating Offshore Wind Turbines." Ph.D. dissertation, Norwegian University of Science and Technology. <http://ntnu.diva-portal.org/smash/record.jsf?pid=diva2:348860>.
- Massel, Stanisław R. 2001. "Wavelet analysis for processing of ocean surface wave records." *Ocean Engineering* 28: 957-987.
- Matha, Denis, Frank Sandner, and David Schlipf. 2014. "Efficient critical design load case identification for floating offshore wind turbines with a reduced nonlinear model." <http://stacks.iop.org/1742-6596/555/i=1/a=012069?key=crossref.2cf58ea90e06a51553c9c6441bd0248d>.

- Matha, Denis, Markus Schlipf, Ricardo Pereira, and Jason Jonkman. 2011. "Challenges in Simulation of Aerodynamics, Hydrodynamics , and Mooring-Line Dynamics of Floating Offshore Wind Turbines." *21st Offshore and Polar Engineering Conference Maui, Hawaii*.
- Mathworks. 2016. "Global Optimization Toolbox: User's Guide (R2016b)."
- Molins, Climent, Alexis Campos, Frank Sandner, and Denis Matha. 2014. "Monolithic Concrete Off-Shore Floating Structure For Wind Turbines." *Proceedings of the EWEA*.
- Montgomery. 2013. *Design and Analysis of Experiments*.
- Morison, J. R. 1953. "The Force Distribution Exerted by Surface Waves on Piles." Tech. rep., Institute of Engineering Research, Wave Research Laboratory.
- Myhr, Anders, and Tor Anders Nygaard. 2012. "Load Reductions and Optimizations on Tension-Leg-Buoy Offshore Wind Turbine Platforms." 4: 232-239.
- Müller, Kolja, Frank Lemmer, Friedemann Borisade, Matthias Kretschmer, Julia Gruber, Lina Hagemann, Ngoc-Do Nguyen, and Luca Vita. 2015. "LIFES50+ D7.4 State-of-the-Art FOWT design practice and guidelines." Tech. rep., University of Stuttgart. http://lifes50plus.eu/wp-content/uploads/2015/11/GA_640741_LIFES50_D7.4.pdf.
- Müller, Kolja, Mario Reiber, and Po Wen Cheng. 2016. "Comparison of Measured and Simulated Structural Loads of an Offshore Wind Turbine at Alpha Ventus." *International Journal of Offshore and Polar Engineering*.
- Müller, Kolja, Martin Dazer, and Po Wen Cheng. 2017. "Damage Assessment of Floating Wind Turbines Using Latin Hypercube Sampling, In Preparation." *Proceedings Deepwind conference 2017*.
- Raach, Steffen, David Schlipf, Frank Sandner, Denis Matha, and Po Wen Cheng. 2014. "Nonlinear Model Predictive Control of Floating Wind Turbines with Individual Pitch Control." *Proceedings of the American Control Conference*. Portland, Oregon. <http://dx.doi.org/10.18419/opus-3940>.
- Robertson, Amy, Jason Jonkman, M. Masciola, H. Song, Andrew Goupee, Alexander Coulling, and C. Luan. 2014. "Definition of the Semisubmersible Floating System for Phase II of OC4." Tech. rep., NREL, Boulder/USA. <http://www.nrel.gov/docs/fy14osti/60601.pdf>.
- Ruiter, Marten Jan De. 2015. "Integrated Automated Optimization of Offshore Wind Turbine and Support Structure Far and Large Offshore wind." *EERA Deepwind*. Trondheim/NO. http://www.sintef.no/Projectweb/Deepwind_2015/Presentations/.
- Sandner, Frank, David Schlipf, Denis Matha, and Po Wen Cheng. 2014. "Integrated Optimization Of Floating Wind Turbine Systems." *Proceedings of the ASME 33rd International Conference on Ocean, Offshore and Arctic Engineering*. San Francisco, Francisco. doi:10.1115/OMAE2014-24244.
- Sandner, Frank, David Schlipf, Denis Matha, Robert Seifried, and Po Wen Cheng. 2012. "Reduced Nonlinear Model of a Spar-Mounted Floating Wind Turbine." *Proceedings of the German Wind Energy Conference DEWEK*. Bremen, Germany. <http://dx.doi.org/10.18419/opus-4528>.

- Sandner, Frank, Wei Yu, and P. W. Cheng. 2015. "Parameterized Dynamic Modelling Approach for Conceptual Dimensioning of a Floating Wind Turbine System." *EERA Deepwind*. Trondheim/NO. http://www.sintef.no/globalassets/project/eera-deepwind-2015/presentations/e/e2_sandner_univ-stuttgart.pdf.
- Sandner, Frank, Wei Yu, Denis Matha, José Azcona, Xabier Munduate, Enrique Grela, Spyros Voutsinas, and Anand Natarajan. 2014. "INNWind.EU D4.33: Innovative Concepts for Floating Structures." Tech. rep.
- Schafhirt, Sebastian, Daniel Zwick, and Michael Muskulus. 2014. "Topology Optimization of a Jacket Structure for an Offshore Wind Turbine with a Genetic Algorithm." *Journal of Ocean and Wind Energy* 1: 209-216.
- Schlipf, David, Eric Simley, Frank Lemmer, Lucy Pao, and Po Wen Cheng. 2015. "Collective Pitch Feedforward Control of Floating Wind Turbines Using Lidar." *Journal of Ocean and Wind Energy* 2: 223-230. doi:10.17736/jowe.2015.arr04.
- Schlipf, David, Frank Sandner, Steffen Raach, Victor Hocke, Denis Matha, and Po Wen Cheng. 2013. "Nonlinear Model Predictive Control of Floating Wind Turbines." http://elib.uni-stuttgart.de/opus/volltexte/2013/8516/pdf/13TPC_987Schlipf.pdf.
- Siebertz, Karl, David Van Bebber, and Thomas Hochkirchen. 2010. *Statistische Versuchsplanung: Design of Experiments (DoE)*. Springer.
- Skogestad, S., and I. Postlethwaite. 2007. *Multivariable feedback control: Analysis and design*. Chichester: John Wiley and Sons.
- Wang, Shan. 2007. "Review of Metamodeling Techniques in Support of Engineering Design Optimization." *Journal of Mechanical Design*.
- Yu, Wei. 2014. "Conceptual Design of an Innovative Floating Platform for Large Offshore Wind Turbines." study project, University of Stuttgart.